

Petrology, Age and Geodynamic Implication of the Panafrican Granitoids Associated with the Glito-Kpatala Shear Zone (South-East Togo)

Gnanwasou Alayi^{1*}, Sarakawa Abalo Malibida Kpanzou¹, Yao Agbossoumondé¹, Essodina Padaro¹, René-Pierre Menot², Mahaman Sani Tairou¹

¹Département de Géologie, Faculté des Sciences, Université de Lomé, Lomé, Togo

²Laboratoire Magmas et Volcans, Université Jean Monnet, Saint Etienne, France

Email: *agnanwasou@yahoo.fr

How to cite this paper: Alayi, G., Kpanzou, S.A.M., Agbossoumondé, Y., Padaro, E., Menot, R.-P. and Tairou, M.S. (2023) Petrology, Age and Geodynamic Implication of the Panafrican Granitoids Associated with the Glito-Kpatala Shear Zone (South-East Togo). *International Journal of Geosciences*, 14, 1193-1225.

<https://doi.org/10.4236/ijg.2023.1412061>

Received: November 27, 2023

Accepted: December 26, 2023

Published: December 29, 2023

Copyright © 2023 by author(s) and Scientific Research Publishing Inc.

This work is licensed under the Creative Commons Attribution International License (CC BY 4.0).

<http://creativecommons.org/licenses/by/4.0/>



Open Access

Abstract

The granitic plutons associated with the Glito-Kpatala shear zone are composed of biotite and amphibole granodiorites, biotite granites, two-mica granites and aplitic granites, which are very poorly represented. The chemical and mineralogical compositions of these facies indicate that they are I type and belong to high-K calc-alkaline series, with a chemical metaluminous character displayed by the granodiorites relative to the biotite and two-mica facies whose chemical compositions vary between metaluminous and peraluminous character. The Th/Ta (14.04 - 43.82 ppm, mean = 26.05), Th/U (2.58 to 15.05 ppm, mean = 5.85 ppm), Zr/Hf (25.27 to 37.21, mean = 30.67 ppm) and Rb/Sr (0.16 to 4.32; mean = 1.67 ppm) ratios of these granitoids reveal a strong crustal involvement in their magmatogenesis. Variations in CaO/Na₂O (0.47 - 1.44 ppm), Rb/Sr (0.14 - 0.27 ppm), Rb/Ba (0.07 - 0.14 ppm) and Sr/Y (38.21 - 174.42 ppm) ratios indicate that biotite and amphibole granodiorites with their excessive Ni (135.37 - 139.51 ppm) and Cr (395.73 - 447.74 ppm) were derived from a mafic to intermediate lower continental crust where garnet and/or amphibole were stable residual assemblage minerals. The moderate Sr/Y ratios (1.81 - 9.47 ppm) and low transition elements Ni (1 - 6.44 ppm) and Cr (7.89 - 13.47 ppm) contents in both the two-mica and biotite granites are consistent with their emplacement at relatively shallow depths in the upper to mean continental crust, at pressures below 10 Kbar. In the two-mica granites, moderate CaO/Na₂O (0.20 - 0.57 ppm, mean = 0.38 ppm) and Rb/Ba (0.39 - 1.37, mean = 0.84 ppm) ratios and quite varied Rb/Sr (1.53 - 4.23 ppm, mean = 2.85 ppm) ratios indicate a predominant derivation from psammitic and

pelitic metasediments rather than metagreywackes. These low ratios ($0.25 \leq \text{CaO}/\text{Na}_2\text{O} \leq 0.32$, mean = 0.28 ppm; $0.31 \leq \text{Rb}/\text{Ba} \leq 0.44$, mean = 0.39 ppm; $1.11 \leq \text{Rb}/\text{Sr} \leq 1.78$, mean = 0.39 ppm) in biotite granites are more consistent with melting from a metagreywacke-derived source. Evidence for the contribution of mantle-derived mafic magma with granitic magma in the plutons studied is materialized by the presence of magmatic enclaves in both granodiorites and two-mica granites, the volcanic arc geochemical signatures displayed by the plutons in geotectonic diagrams and Nb/Ta ratios (14.14 - 34.61 ppm) closer to mantle estimates. Geochemical data and radiometric dating elements suggest that the granitoids studied can be integrated into the pan-African late magmatic episode, which corresponds between 606 and 583 Ma, to the activity of transcurrent ductile strike-slips and to the synchronous emplacement of high K calc-alkaline plutons in a post-collisional context.

Keywords

Pan-African Granitoids, Post-Collisional, Shear Zone, South-East Togo

1. Introduction

The granitoids associated with the Glito-Kpatala shear zone in south-east Togo (**Figure 1**), are part of the plutonic units outcropping on the western front of the inner zone of the pan-African Dahomeyide chain. The Dahomeyides chain is the result of a collision between the passive margin of the West African craton and the entire Benin-Nigerian eastern thrust plate and the Tuareg shield [1] [2]. The granitic plutons identified in this zone or Benino-Nigerian peneplain are generally eburnean (c. 2000 Ma) [3] and especially Pan-African (c. 650 - 550 Ma) [4] [5]. A few ring complexes of anorogenic granites of Carboniferous to Cretaceous age (“younger granites”) [6] and Cenozoic age are also found in the east of the province in Nigeria. The shear zone bordering the western front of the plutons studied corresponds to dextral deformation that produced blasto to ultra-mylonitic corridors several kilometers thick [7]. It represents the continuation of the transcontinental shears that delimit the main structural domains of the Hoggar, extending into the Adrar of Iforas to reach the basement of the Benino-Togolese plain [7] [8]. In Benin, more recent work by Adissin [8] on several plutons of the Kandi shear zone in the Savalou Dassa region highlights the existence of a succession of calc-alkaline-alkaline magmatic manifestations during transcurrent late to post-collisional deformation. Calc-alkaline magmatic activity is evidenced by the emplacement, in the post-collisional setting, of the Dassa (633 Ma), Gobada (603 ± 10 Ma), Tchetti (607 ± 11 Ma) and Tré (595 ± 12) granites. The emplacement of these plutons preceded the alkaline magmatism represented by the Fita granites (583 ± 9 Ma) [8]. Studies on granitoids in the Togolese part of the peneplain remain general or little known. Indeed, the emplacement chronology of these plutons is not very convincing

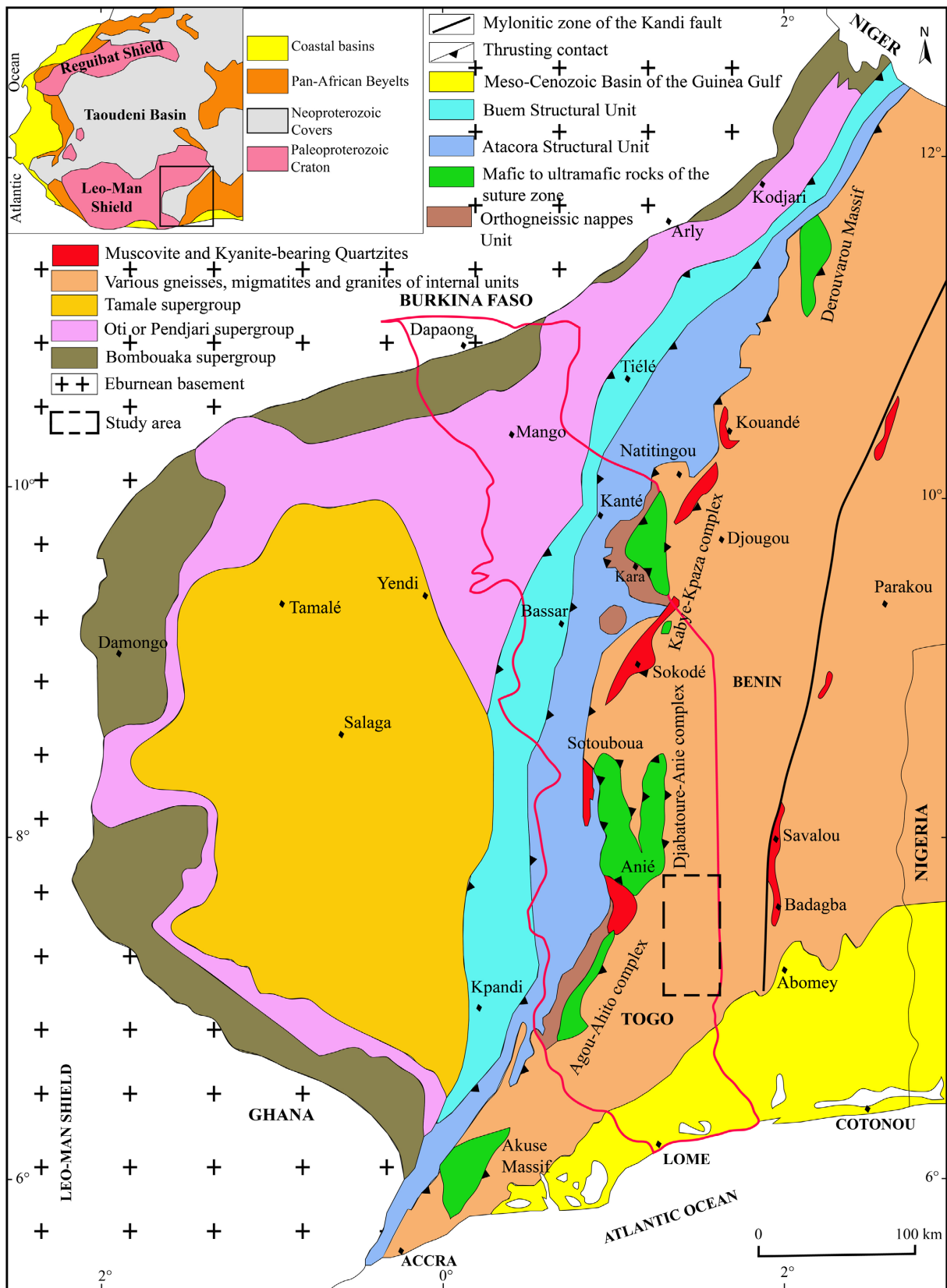


Figure 1. Simplified geological map showing the main structural domains of the Pan-African Dahomeyide belt and its foreland ([9]; slightly modified) with the location of the study area.

because the pan-African ages were assigned on the basis of geochronological data from Benin, Nigeria and the central Hoggar. On the basis of spatial relationships combined with petrographic, geochemical data on minerals and total rocks, and U-Pb dating on zircon, this paper proposes to: 1) determine the nature, age and evolutionary process of the magma of the granitoids studied; 2) propose the petrogenetic model and geodynamic context of emplacement in order to situate these granitoids in the geodynamic evolution of the Pan-African chain in the inner zone.

2. Geological Setting

The granitic plutons associated with the Glito-Kpatala shear zone are part of the geology of the Togolese crystalline basement formed from west to east (**Figure 1**): outer zone units, which include the Buem and Atakora structural units, the Kpalimé-Amlamé plutono-metamorphic complex and the Kara-Niamtougou orthogneissic formations [9] [10]; suture zone units, formed by a submeridian alignment of basic to ultrabasic massifs [11] [12] [13] and units of the inner zone corresponding to the peneplain representing the Benino-Nigerian basement composed of gneisso-migmatitic, metasedimentary (schists, marbles and quartzites) and granitoid units [14]. The granitic plutons associated with the Glito-Kpatala shear zone in south-east Togo belong to the latter unit. These plutons are organized into chains of elliptical intrusions trending NNE-SSW (**Figure 2**), the same as the shear zone. Strongly affected by the shear zone, the immediate host of the plutons is composed of migmatites, bedded amphibolites and biotite and amphibole gneissic formations from west to east (**Figure 2**). A series of radiometric analyses carried out on the surrounding formations [3] gives an Eburnean age (1708 ± 169 Ma) for the Agbélouvé migmatitic orthogneisses and a Pan-African age for the Kpédomé migmatites (528 ± 24 Ma). These plutons were chosen for study because: 1) their proximity with those in the center of Benin that have been studied in great detail [8] [15] and 2) the ease of access to these plutons.

3. Analytical Method

On the basis of petrographic studies, eight samples, including two (2) granodiorites, five (5) granites and one (1) aplite representative of the plutons studied, were selected for geochemical analyses (major elements, trace elements and rare earths) on total rock. The GPS (Global positioning system) locations of the samples taken are given in **Table 1**. The analyses were carried out at the LMV laboratory (Magmas and Volcanoes Laboratory) of the University of Auvergne (Clermont-Ferrand, France) using a ULTIMA-C ICP-AES (Inductively Coupled Plasma-Atomic Emission Spectroscopy) laser. The analytical results are reported in **Table 2**. The chemical composition of the main mineral phases in the samples analyzed was determined by electron microprobe on thin section. The equipment used was a Cameca SX-100 electron microprobe from the CNRS

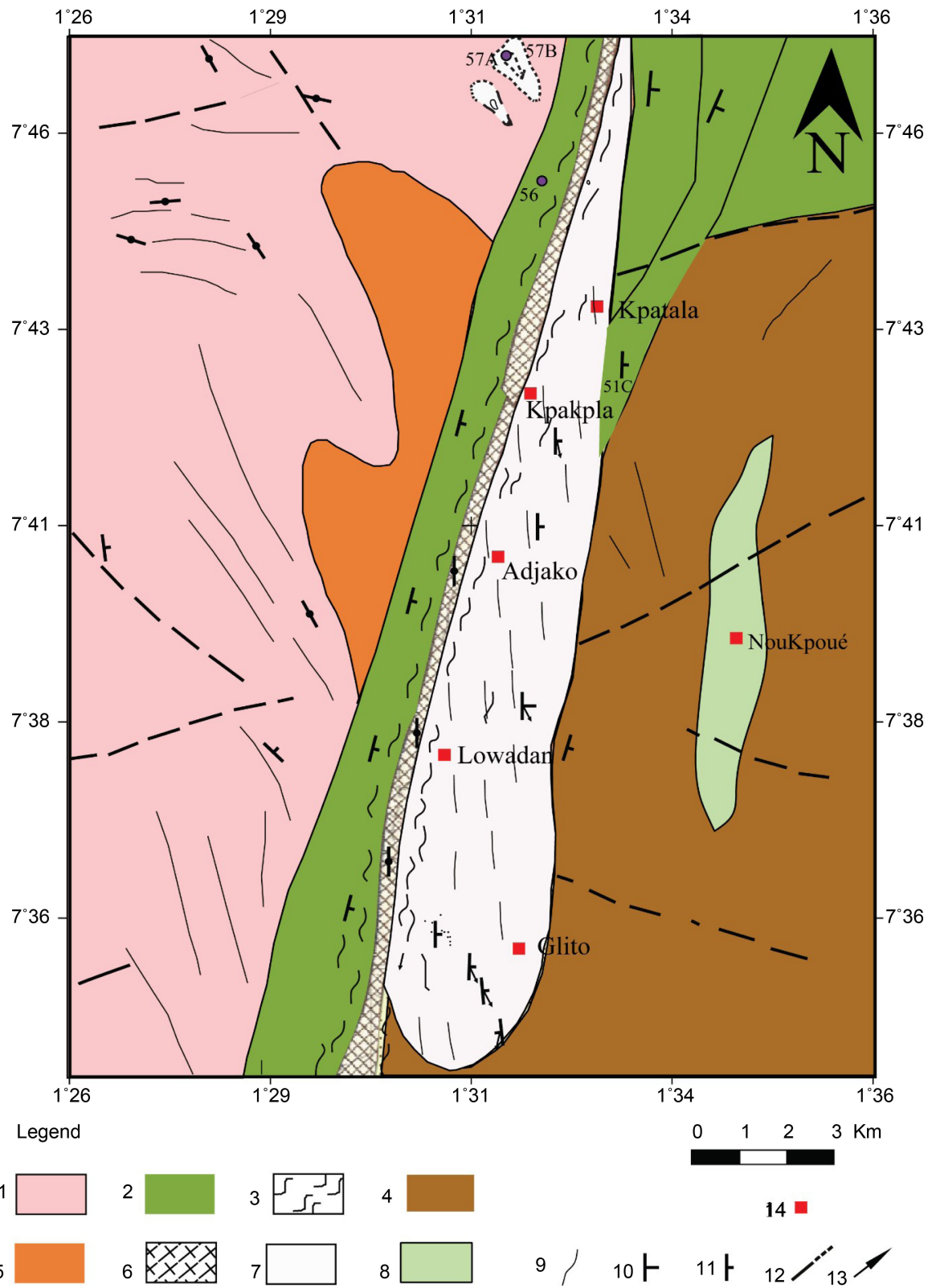


Figure 2. Geological and structural map of the study area showing sampled localities. 1: Migmatites; 2: Foliated amphibolites and amphibolitic gneisses; 3: Mylonitic to cataclastic facies; 4: Biotite and amphibole gneissic formations; 5: Suboutcrop of two micas and garnet-bearing gneiss; 6: Shear zone; 7: Granite massifs; 8: Granodiorites; 9: Traces of foliation; 10: $30 < \text{Dip} < 60$; 11: $60 < \text{Dip} < 90$; 12: Fractures; 13: Lineations; 14: Locality sampled.

Table 1. Main characteristics of the granitoids of southeast Togo.

Petrographic facies	biotite and amphibole Granodiorite	Biotite Granite	2-micas Granite	Aplite
No. of samples analyzed	47C; 51C	9A; 55C; 55D	10C; 10D	10B
GPS coordinates	07°38'31.5"N 001°32'11.7"E	07°40'48.2"N 001°31'19.7"E	07°34'40.1"N 001°31'18.9"E	07°35'20.2"N 001°30'46.2"E
Locality	NouKpoué	Adjako	Glito	Glito
Magmatic enclaves	Rare enclaves of diorite	Virtually no diorite enclaves	Rare enclaves of diorite	Absent
Metamorphic enclaves	Absent	Rare enclaves of gneiss	Rare enclaves of gneiss	Absent
Feldspar	Oligoclase to Andesine (An ₁₆₋₄₃); Orthoclase (Or ₉₂₋₉₃)	Perthitic Orthoclase (Or ₈₇₋₉₇); Albite to Oligoclase (An ₁₋₁₆)	Perthitic Orthoclase (Or ₉₂₋₉₇); Albite to Oligoclase (An ₁₋₂₆)	Microcline (Or ₉₄₋₉₇); Albite (An ₂₋₄)
Ferromagnesian	Magnesian biotite (0.37 ≤ X _{Fe} ≤ 0.40) Calcium amphibole (0.69 ≤ X _{Mg} ≤ 0.77)	Ferriferous biotite (0.75 ≤ X _{Fe} ≤ 0.81)	Ferriferous biotite (0.72 ≤ X _{Fe} ≤ 0.93) Muscovite (0.01 ≤ Ti ≤ 0.07) (0.32 ≤ Mg ≤ 0.38)	Quite rare biotite and muscovite
Accessory minerals	Zircon; Epidote; titanite	Zircon	Muscovite; Epidote; Zircon; Apatite	Epidote; chlorite; zircon

LMV laboratory (Laboratoire Magmas et Volcans) at the University of Auvergne (Clermont-Ferrand, France). The phases analysed were the key minerals in granitoids: plagioclase, biotite and amphibole. Structural formulae were calculated on the basis of 8 oxygens for feldspars, 22 oxygens for biotites and 23 oxygens for amphiboles. The results of representative chemical analyses of the mineral phases are reported in **Table 3** and **Table 4**. U-Pb dating analyses on zircon were carried out on 2 granite samples (**Table 5**). The selected samples were prepared at the Geochronological Research Centre of the University of São Paulo, Brazil, for in situ U-Pb analysis on zircons by laser ablation with inductively coupled plasma-mass spectrometry (LA-ICP-MS). The age was calculated using Isoplot software version 3.16 [16].

4. Results

4.1. Petrography and Mineralogy

Field observations coupled with thin section studies have enabled us to identify four petrographic types: biotite and amphibole granodiorites, biotite granites, two-mica granites and aplitic granites, most of which are found in the form of

Table 2. Results of geochemical analyses of representative samples of plutons studied.

Type of rocks	biotite and amphibole granodiorite		2-micas granite			biotite granite		
Sample	47C	51C	10C	10D	10B	09A	55C	55D
SiO ₂ (%)	63.72	62.29	72.94	74.81	72.83	73.80	72.74	72.82
Al ₂ O ₃	14.63	14.60	14.46	13.72	14.92	13.36	14.09	14.34
Fe ₂ O ₃ t	5.02	5.63	1.61	1.51	1.58	2.27	2.50	2.11
MgO	4.75	5.40	0.29	0.19	0.38	0.24	0.41	0.37
CaO	4.29	4.93	1.54	0.87	2.30	0.97	1.15	1.08
Na ₂ O	3.80	3.43	3.98	4.39	4.02	3.81	3.65	3.87
K ₂ O	2.97	2.83	4.88	4.27	3.70	5.19	5.05	5.03
TiO ₂	0.59	0.62	0.20	0.15	0.19	0.25	0.27	0.25
MnO	0.08	0.09	0.04	0.05	0.03	0.04	0.05	0.04
P ₂ O ₅	0.15	0.18	0.06	0.05	0.05	0.08	0.09	0.10
Total	100.00	100.00	100.00	100.00	100.00	100.00	100.00	100.00
Rb (ppm)	88.62	85.08	345.82	367.49	272.25	208.31	179.48	240.82
Ba	946.26	873.90	451.08	267.54	690.32	474.13	586.83	584.75
Nb	7.95	7.73	19.36	24.46	9.88	19.14	12.89	18.77
Ta	0.23	0.25	1.54	1.69	0.94	1.14	0.49	1.33
Sr	539.35	544.37	123.37	86.86	177.53	117.09	161.18	149.43
Zr	46.03	34.24	123.99	115.58	85.87	235.75	171.76	204.14
Y	13.97	14.25	34.46	47.91	18.75	22.69	17.09	23.60
Hf	1.52	1.32	4.58	4.57	2.98	6.85	4.62	5.62
Ni	135.37	139.51	1.78	1.01	3.35	1.00	6.44	1.65
Cr	395.73	447.74	13.18	10.91	10.59	13.47	7.89	11.44
V	87.92	93.97	7.07	5.68	9.84	6.67	7.54	10.31
U	1.84	2.06	9.38	9.19	4.30	4.25	1.42	3.49
Th	9.09	8.13	27.22	23.68	15.04	29.75	21.42	24.24
Sc	11.53	12.44	1.05	1.10	0.99	1.56	1.51	2.87
Co	19.22	20.47	1.93	1.44	2.71	2.09	2.44	2.15
Cu	24.73	43.20	3.05	4.75	6.28	8.37	2.98	6.75
Zn	57.99	103.00	43.69	50.49	43.21	49.80	48.97	45.46
Cs	4.22	4.19	8.94	11.64	8.23	3.03	1.74	6.77
La (ppm)	32.86	30.72	27.84	23.86	18.66	62.52	62.15	56.97
Ce	61.85	57.90	56.93	49.06	33.21	111.10	111.37	100.23
Pr	6.60	6.32	6.40	5.53	3.89	11.64	11.62	10.50
Nd	23.89	23.36	23.34	20.60	13.78	39.40	39.13	35.61
Sm	4.18	4.16	5.21	4.97	2.86	6.49	6.18	6.17

Continued

Eu	1.04	1.07	0.52	0.43	0.48	0.85	0.94	0.76
Gd	3.20	3.22	4.66	5.14	2.67	4.82	4.36	4.66
Tb	0.47	0.47	0.80	0.93	0.44	0.73	0.62	0.72
Dy	2.48	2.50	4.84	6.00	2.65	3.83	3.09	3.81
Ho	0.46	0.48	0.99	1.25	0.52	0.74	0.57	0.72
Er	1.33	1.35	3.08	4.02	1.65	2.21	1.61	2.11
Tm	0.20	0.20	0.52	0.70	0.28	0.34	0.24	0.32
Yb	1.26	1.27	3.76	4.91	2.00	2.30	1.49	2.18
Lu	0.18	0.18	0.56	0.74	0.30	0.35	0.22	0.33
Eu/Eu*	0.85	0.88	0.32	0.25	0.52	0.45	0.54	0.42
(La)N	85.56	80.00	72.49	62.12	48.60	162.82	161.84	148.36
(Sm)N	18.05	17.97	22.49	21.48	12.36	28.00	26.67	26.66
(Gd)N	10.45	10.52	15.21	16.76	8.72	15.71	14.24	15.22
(Yb)N	5.50	5.53	16.34	21.35	8.69	9.98	6.48	9.48
(La/Sm)N	4.74	4.45	3.22	2.89	3.93	5.81	6.07	5.57
(Gd/Yb)N	1.90	1.90	0.93	0.79	1.00	1.57	2.20	1.60
(La/Yb)N	15.57	14.47	4.44	2.91	5.59	16.31	24.99	15.64
ΣREE	140.01	133.22	139.45	128.14	83.40	247.31	243.58	225.09

veins in two-mica granites. The main characteristics of these petrographic facies are summarized in **Table 1**.

4.1.1. Biotite and Amphibole Granodiorites

These facies lie to the east of the biotite and two-mica facies (**Figure 2**) and can be seen in massive banks in the bed of the Noukpoué River (**Figure 3(a)**). The rocks are grey in colour and medium to fine grained. They have an oriented structure and are distinguished by their enrichment in biotite, amphibole and plagioclase. The enclaves observed in these facies are almost entirely magmatic of a dioritic nature and centimetric to decimetric in size, they have undulating contours (**Figure 3(b)**), sometimes ovoid or rounded, suggesting mechanical mixing of magma with their host facies [17]. These rocks are composed of plagioclase, quartz, amphibole, potassic feldspar, biotite, and secondarily zircon, titanite and epidote (**Figure 4(a)** and **Figure 4(b)**). Plagioclases are fairly abundant and show a chemical composition ranging from oligoclase to andesine (**Table 1**; **Figure 5(a)** and **Figure 5(b)**), typical of ACG-type granitoids (amphibole rich calco-Alkaline granite) [18]. The biotite flakes show a magnesian chemical composition ($0.37 \leq X_{Fe} \leq 0.40$) (**Table 1**; **Figure 5(d)**) corresponding to phlogopite [19]. These minerals have aluminium ($13.90 \leq \% \text{Al}_2\text{O}_3 \leq 16.59$), magnesium ($8.44 \leq \% \text{MgO} \leq 14.10$) and FeO/MgO ratios ($1.06 \leq \text{FeO/MgO} \leq$

Table 3. Representative chemical composition of amphiboles, biotites and muscovites of the studied plutons.

Minerals	Amphibole						Biotite				Muscovite					
Type of rocks	biotite and amphibole granodiorite						biotite granite				2 micas granites					
Sample	47C	47C	51C	51C	47C	51C	51C	09A	55C	55D	10A	10C	10D	10C	10D	10D
SiO ₂	55.16	51.91	55.27	50.81	37.78	37.46	37.74	35.45	34.82	34.15	33.6	36.81	35.75	47.27	46.2	45.86
TiO ₂	0.07	0.3	0.08	0.54	1.71	1.5	2.19	1.82	2.3	1.9	2.42	1.27	1.78	0.2	0.35	0.38
Al ₂ O ₃	1.65	4.08	1.67	5.18	15.92	15.81	15.68	16.29	16.45	15.8	16.2	17.68	16.44	30.05	30.7	29.66
Cr ₂ O ₃	0.03	0.15	0.01	0.2	0.17	0.13	0.19	0	0	0	0.03	0	0.02	0.03	0	0.04
FeOt	9.64	11.4	9.4	11.75	15.68	15.33	14.92	27.36	27.46	28.13	30.3	24.02	25.73	5.29	6.25	6.2
MnO	0.32	0.26	0.31	0.3	0.27	0.2	0.23	0.49	0.45	0.45	0.77	0.55	0.89	0.08	0.07	0.11
MgO	17.29	15.15	17.39	14.92	13.31	13.44	14.1	4.32	3.72	4.21	1.34	5.16	3.81	1.9	0.58	0.6
CaO	12.74	12.63	12.61	12.47	0	0	0	0.05	0.03	0.02	0	0.03	0.01	0	0	0
Na ₂ O	0.21	0.43	0.2	0.64	0.06	0.02	0.04	0	0.06	0.06	0.03	0.04	0.05	0.21	0.18	0.16
K ₂ O	0.07	0.3	0	0.44	9.87	10.01	9.88	9.79	9.42	9.45	8.75	9.56	9.35	11	10.7	10.95
Total	97.17	96.62	96.93	97.25	94.76	93.9	94.97	95.58	94.71	94.17	93.5	95.11	93.82	96.03	95	93.96
Si	7.86	7.55	7.88	7.38	5.69	5.69	5.66	5.63	5.58	5.55	5.55	5.73	5.73	6.4	6.33	6.38
Ti	0.01	0.03	0.01	0.06	0.19	0.17	0.25	0.22	0.28	0.23	0.3	0.15	0.21	0.02	0.04	0.04
Al IV	0.14	0.45	0.12	0.62	2.31	2.31	2.34	2.37	2.42	2.45	2.45	2.27	2.27	1.6	1.67	1.62
Al VI	0.14	0.25	0.16	0.26	0.52	0.53	0.43	0.68	0.7	0.58	0.71	0.98	0.84	3.19	3.3	3.24
Al tot	0	0.02	0	0.02	2.83	2.83	2.77	3.05	3.11	3.03	3.16	3.25	3.11	4.79	4.97	4.86
Cr	1.15	1.39	1.12	1.43	0.02	0.02	0.02	0	0	0	0	0	0	0	0	0
Fe ²⁺	0.04	0.03	0.04	0.04	1.98	1.95	1.87	3.64	3.68	3.82	4.19	3.13	3.45	0.6	0.72	0.72
Mn	3.67	3.28	3.69	3.23	0.03	0.03	0.03	0.07	0.06	0.06	0.11	0.07	0.12	0.01	0.01	0.01
Mg	1.95	1.97	1.93	1.94	2.99	3.05	3.15	1.02	0.89	1.02	0.33	1.2	0.91	0.38	0.12	0.13
Na	0.06	0.12	0.05	0.18	0.02	0.01	0.01	0	0.02	0.02	0.01	0.01	0.02	0.06	0.05	0.04
K	0.01	0.06	0	0.08	1.9	1.94	1.89	1.99	1.93	1.96	1.84	1.9	1.91	1.9	1.88	1.94
Total	15.03	15.15	15	15.24	15.65	15.68	15.65	15.61	15.55	15.69	15.5	15.44	15.46	14.16	14.1	14.13
Fe/(Fe ²⁺ + Mg)	0.76	0.7	0.77	0.69	0.4	0.39	0.37	0.78	0.81	0.79	0.93	0.72	0.79	0.61	0.86	0.85

2.76) similar to calc-alkaline granitoids from orogenic zones [20]. The amphiboles are magnesian ($14.75 \leq \text{MgO} \leq 17.39$) and calcic ($\text{CaB} \geq 1.5$) with a chemical composition ranging from magnesiohornblende to actinolite (Table 1, Figure 5(c)) [21].

4.1.2. Biotite and Two-Mica Granites

These facies form a chain of hills (Figure 2; Figure 3(c)) aligned NNE-SSW.

Table 4. Representative chemical composition of feldspars of studied plutons.

Type of rocks	biotite and amphibole granodiorite				2 micas granites			biotite granite			
Sample	51C	51C	47C	47C	10C	10C	10D	55C	09A	55C	55C
SiO ₂	64.38	63.31	63.37	56.65	64.11	61.4	64.59	65.26	64.59	64.53	60.45
Al ₂ O ₃	22.8	18.7	18.66	26.71	17.87	22.84	17.95	18.66	18.26	18.43	20.93
FeO	0	0	0.01	0	0.04	0.08	0	0.03	0	0.02	0.36
CaO	3.22	0.02	0.01	8.81	0	5.22	0	0	0	0	3.07
Na ₂ O	9.52	0.73	0.82	6.28	0.33	8.09	0.93	1.53	0.4	0.9	8.58
K ₂ O	0.07	15.48	15.2	0.15	16.5	0.15	15.49	14.88	16.75	15.77	0.26
Total	99.99	99.22	99.87	98.64	98.84	97.76	98.96	100.54	99.99	99.79	93.74
Si	2.83	2.97	2.97	2.57	3	2.78	3.01	2.99	2.99	2.99	2.84
Al	1.18	1.03	1.03	1.43	0.99	1.22	0.99	1.01	1	1.01	1.16
Fe ²⁺	0	0	0	0	0	0	0	0	0	0	0.01
Ca	0.15	0	0	0.43	0	0.25	0	0	0	0	0.15
Na	0.81	0.07	0.07	0.55	0.03	0.71	0.08	0.14	0.04	0.08	0.78
K	0	0.93	0.91	0.01	0.99	0.01	0.92	0.87	0.99	0.93	0.02
Total	4.98	5.01	5.01	4.99	5.01	4.97	5	5.01	5.02	5.01	4.97
Or	0	0.93	0.92	0.01	0.97	0.01	0.92	0.87	0.97	0.92	0.02
Ab	0.84	0.07	0.08	0.56	0.03	0.73	0.08	0.13	0.03	0.08	0.82
An	0.16	0	0	0.43	0	0.26	0	0	0	0	0.16

Located at the southern end of the chain, the two-mica facies form the biggest hills in the neighborhood of Glito, while the biotite facies are organized into small hills stretching from Lowadan to Kpatala via Adjako and Kpakpla. In outcrop, the fairly deformed biotite granites look like orthogneiss in places. Pinkish in colour, these facies are almost devoid of enclaves and have a porphyroid texture and oriented structure (**Figure 3(d)**). Their crystalline base is fairly enriched in quartzo-feldspathic minerals, and is formed of regularly oval crystals of feldspar and quartz, around which the ferromagnesians, formed of biotite sheets (**Figure 3(d)**). Compared with the previous facies, the two-mica facies are only slightly deformed. Light grey in colour, they have a normal grained to porphyroid texture and contain two types of enclaves: dioritic enclaves with rounded to ovoid contours, centimetric to decimetric in size and showing fairly sharp margins with their host facies (**Figure 3(e)**) and centimetric panels of orthogneiss with angular margins (**Figure 3(f)**). Apart from muscovite, which is found in the two-mica facies (**Figure 4(c)** and **Figure 4(d)**), the biotite and two-mica granites share a common mineralogical composition consisting of quartz, potassium feldspar, plagioclase and biotite. Accessory minerals include zircon, apatite, allanite, sphene and epidotes (**Figures 4(c)-(f)**). Plagioclase composition ranges from albite to oligoclase, but is more restricted in the biotite granites (An₂₋₁₈) than in the two-mica granites (An₁₋₂₆) (**Table 1; Figure 5(a)** and

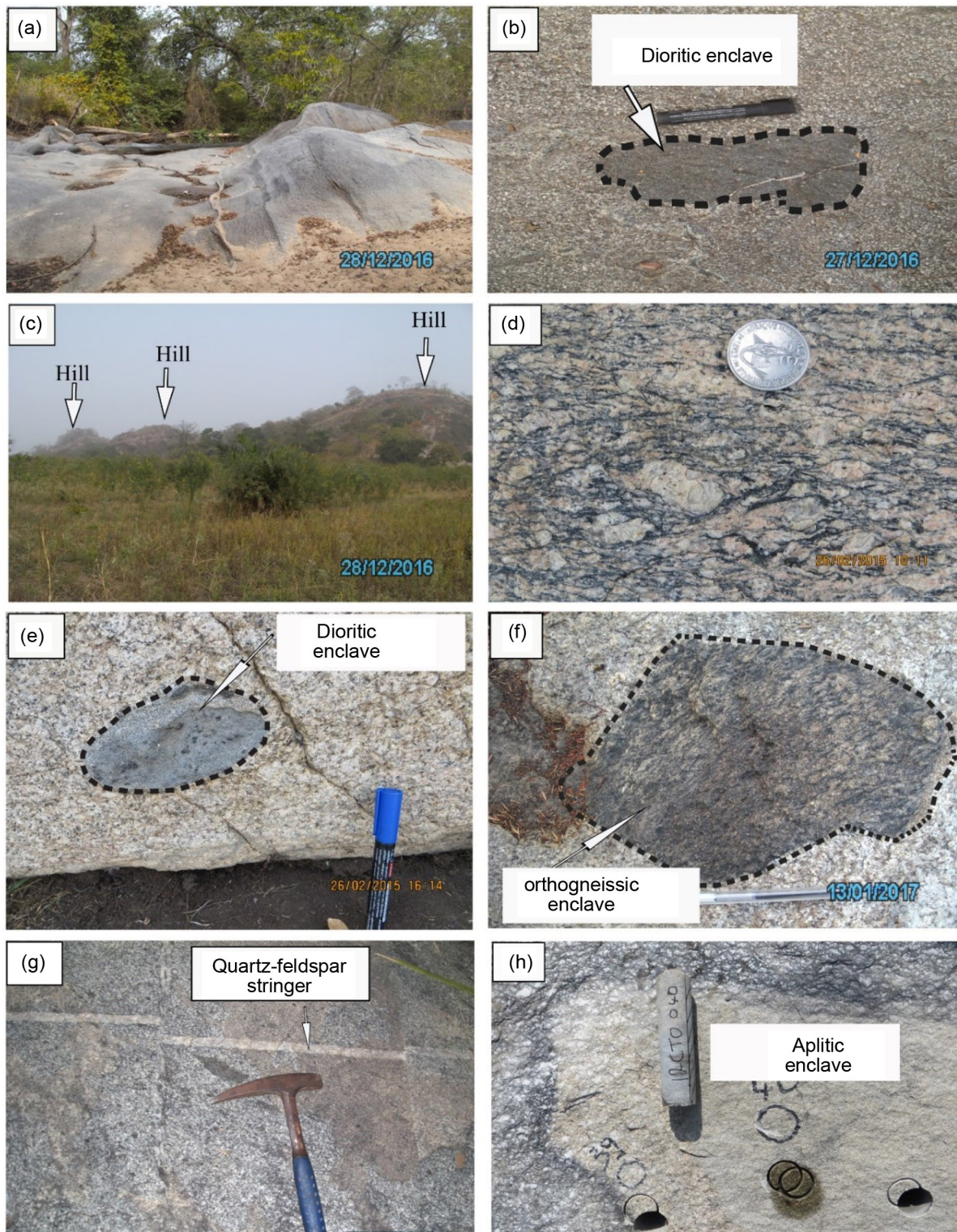


Figure 3. Field photograph of the granitoids studied. (a) aspect of the granodiorites outcrop in the streambed of Noukpoué River ($07^{\circ}38'31.5''\text{N}$, $001^{\circ}32'11.7''\text{E}$); (b) magmatic enclave of dioritic in granodiorites; (c) hills range composed of biotite granite ($07^{\circ}40'48.2''\text{N}$; $001^{\circ}31'19.7''\text{E}$); (d) appearance of the biotite granites of Adjako ($07^{\circ}40'48.2''\text{N}$; $001^{\circ}31'19.7''\text{E}$); (e) dioritic enclave in the two-micas granites of Glito (GPS: $07^{\circ}34'40.1''\text{N}$, $001^{\circ}31'18.9''\text{E}$); (f) enclave of orthogneiss in the two-micas granites of Glito ($07^{\circ}34'58.8''\text{N}$, $001^{\circ}31'12.4''\text{E}$); (g), (h) string and aplitic enclave in two-micas granites ($07^{\circ}34'58.8''\text{N}$, $001^{\circ}31'12.4''\text{E}$).

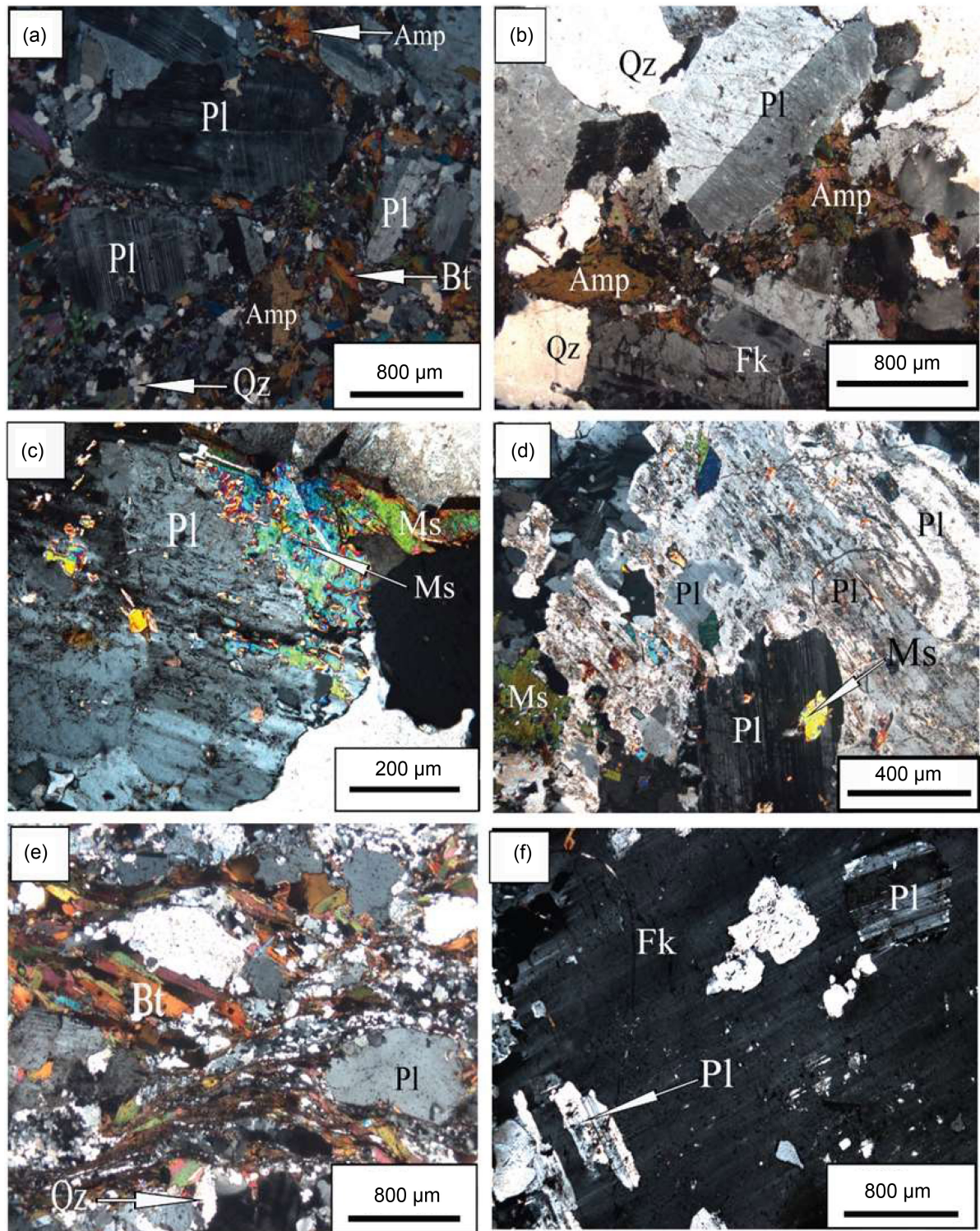


Figure 4. Microphotograph of thin sections representative of the studied granitoids. (a) appearance of the biotite and amphibole granodiorites of Noukpoué showing a phenocrystal of plagioclase (Pl) with corroded edges; (b) appearance of biotite and amphibole granodiorites revealing automorphic to subautomorphic crystals of potassium feldspar (Fk), plagioclase (Pl), amphibole (Amp) and quartz (Qz); (c) muscovite growing at the expense of plagioclase of Glito's two-micas granites; (d) macled and zoned plagioclases showing alterations in the two-micas granites of Glito; (e) mylonitic texture in the biotite granites of Adjako; (f) phenocrystal of potassium feldspar (Fk) containing automorphic to subautomorphic crystals of plagioclase.

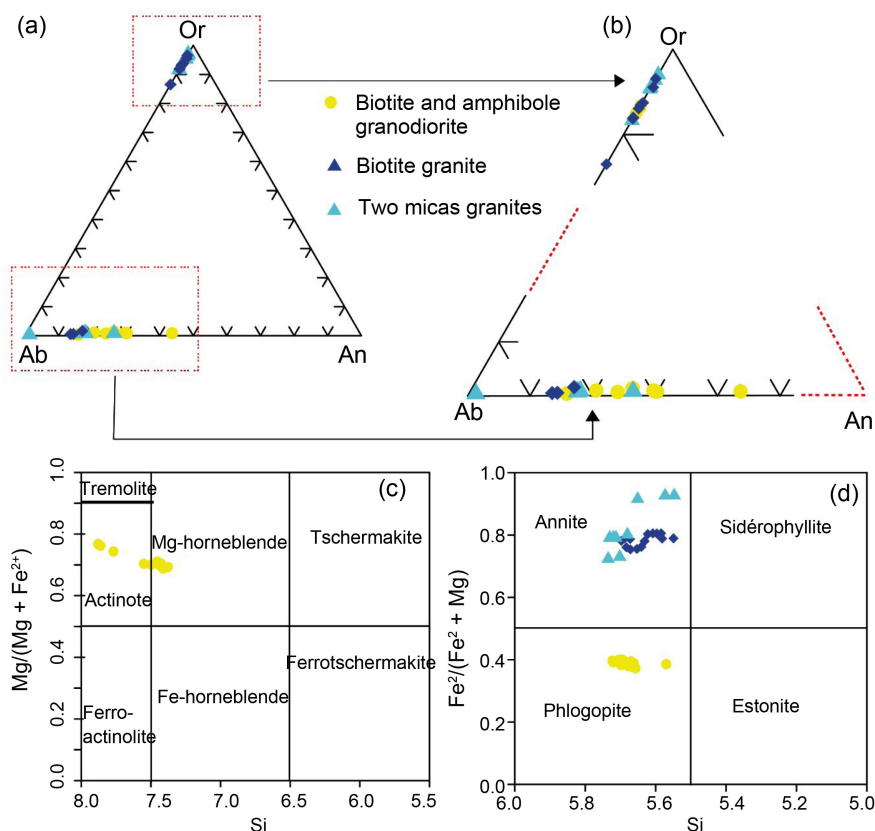


Figure 5. Classification diagrams of feldspars, biotites and amphiboles of the studied granitoids. (a) classification Or (orthoclase)-Ab (albite)-An (anorthite) of feldspars. (b) enlarged version of the feldspar classification diagram. (c) classification Si vs. $Mg/(Mg + Fe^{2+})$ of amphiboles for compositional parameters corresponding to $CaB \geq 1.5$; $(Na + K)A < 0.5$ and $CaA < 0.5$ [21]; (d) classification Si vs. $Fe^{2+}/(Fe^{2+} + Mg)$ of biotites according to [19].

Figure 5(b). These compositional ranges are fairly close to those of KCG-type granites (K rich calco-alkaline granite) [18]. Of variable size, these crystals occur either as small inclusions in potassic feldspar phenocrysts (Figure 4(f)), or as automorphic to subautomorphic sections, zoned or mottled in the crystalline groundmass (Figure 4(c) and Figure 4(d)). The biotite minerals, sometimes chloritized in the facies with two micas, are ferriferous in nature and have a chemical composition corresponding to that of annite (Table 1; Figure 5(d)). These flakes frequently show inclusions of aureate zircon and acicular apatite. The aluminium ($15.13 \leq Al_2O_3 \leq 17.77$) and magnesium ($1.30 \leq MgO \leq 5.16$) contents of these phases are similar to those of peraluminous granitoids from orogenic zones [20]. The potassium feldspars represented by perthitic orthoclase form either large automorphic to subautomorphic crystals sometimes containing plagioclase inclusions (Figure 4(f)); or subautomorphic patches incorporated in the crystalline matrix. The muscovite of the two-mica facies is scarce and occurs as flakes growing at the expense of plagioclase and biotite (Figure 4(d)). Their composition in terms of atomic proportion of Ti ($0.01 \leq Ti \leq 0.07$), Mg ($0.12 \leq Mg \leq 0.35$), Na ($0.03 \leq Na \leq 0.06$), is close to that of secondary muscovite [22].

4.1.3. Aplitic Granites

These facies outcrop either as centimeter-thick quartz-feldspar veins or as enclaves in the two-mica facies (**Figure 3(g)** and **Figure 3(h)**). These rocks are leucocratic, compact with a fine grain size and mainly composed of millimeter-sized grains of quartz and feldspar. The ferromagnesian minerals, biotite and, to a lesser extent, muscovite, are very poorly represented in these rocks. In thin section, the aplitic granites have a mineralogy composed of plagioclase, quartz and potassic feldspars represented by orthoclase and microcline. Biotite is less abundant. Accessory minerals include zircon, epidote, chlorite and muscovite. The plagioclases are of the albite (An_{2-4}) type (**Table 1**) and regularly show signs of destabilization into muscovite. The patches of potassic feldspars, mainly microcline (Or_{94-99}), are fractured and dissected in the crystalline matrix. Biotite, relatively more abundant in enclave facies, forms small lamellae that are often altered to chlorite or destabilized to muscovite.

4.2. Granitoids Geochemistry

The concentrations of major elements expressed in weight percentage (%) and trace elements expressed in parts per million (ppm) of the samples analyzed are shown in **Table 2**.

4.2.1. Major Elements

The SiO_2 content of the granitoids studied ranges from 62.29% to 74.81% (**Table 2**). The biotite and amphibole granodiorites are intermediate in nature ($62.29 \leq \% SiO_2 \leq 63.72$), while the two-mica and biotite facies are purely acidic ($72.74 \leq \% SiO_2 \leq 74.81$). Relative to the biotite and two-mica facies whose major element contents ($0.19 \leq \% MgO \leq 0.41$); $0.87 \leq \% CaO \leq 2.30$; $1.47 \leq \% FeOt \leq 2.44$; $0.15 \leq \% TiO_2 \leq 0.27$; $0.05 \leq \% P_2O_5 \leq 0.10$; $3.70 \leq \% K_2O \leq 5.19$) are comparable, biotite and amphibole granodiorites are characterized by high levels of CaO (4.29 - 4.93 ppm), MgO (4.75 - 5.40 ppm), FeOt (4.90 - 5.50 ppm), TiO_2 (0.59 - 0.62 ppm), P_2O_5 (0.15 - 0.18 ppm) and low levels of K_2O (2.83 - 2.97 ppm). Their Al_2O_3 (14.60 - 14.63 ppm) and Na_2O (3.43 - 3.80 ppm) contents are comparable to those of the biotite and two-mica facies ($13.36 \leq \% Al_2O_3 \leq 14.92$; $3.65 \leq \% Na_2O \leq 4.39$) (**Table 2**). In the SiO_2 vs oxides diagram, of the Harker type [23] (**Figure 6**), both granodiorites and biotite and two-mica granites show an evolutionary trend, with increasing acidity, marked by a negative correlation with the oxides MgO, CaO, TiO_2 , P_2O_5 , FeOt and MnO (**Figure 6(b)**, **Figure 6(c)**, **Figure 6(f)**, **Figures 6(g)-(i)**). The oxides Na_2O , K_2O and Al_2O_3 show an inflection in the biotite and two-mica granites (**Figure 6(a)**, **Figure 6(d)** and **Figure 6(e)**), while the biotite and amphibole granodiorites show a positive correlation with the oxides Na_2O and K_2O and a constant evolutionary trend with the oxide Al_2O_3 (**Figure 6(a)**, **Figure 6(d)** and **Figure 6(e)**). In the Quartz-Feldspar-alkaline-Plagioclase (QAP) normative classification diagram [24], all the samples studied fall within the KCG (K-rich Calc-alkaline Granitoids) and ACG (Amphibole-rich Calc-alkaline Granitoids) granitoids

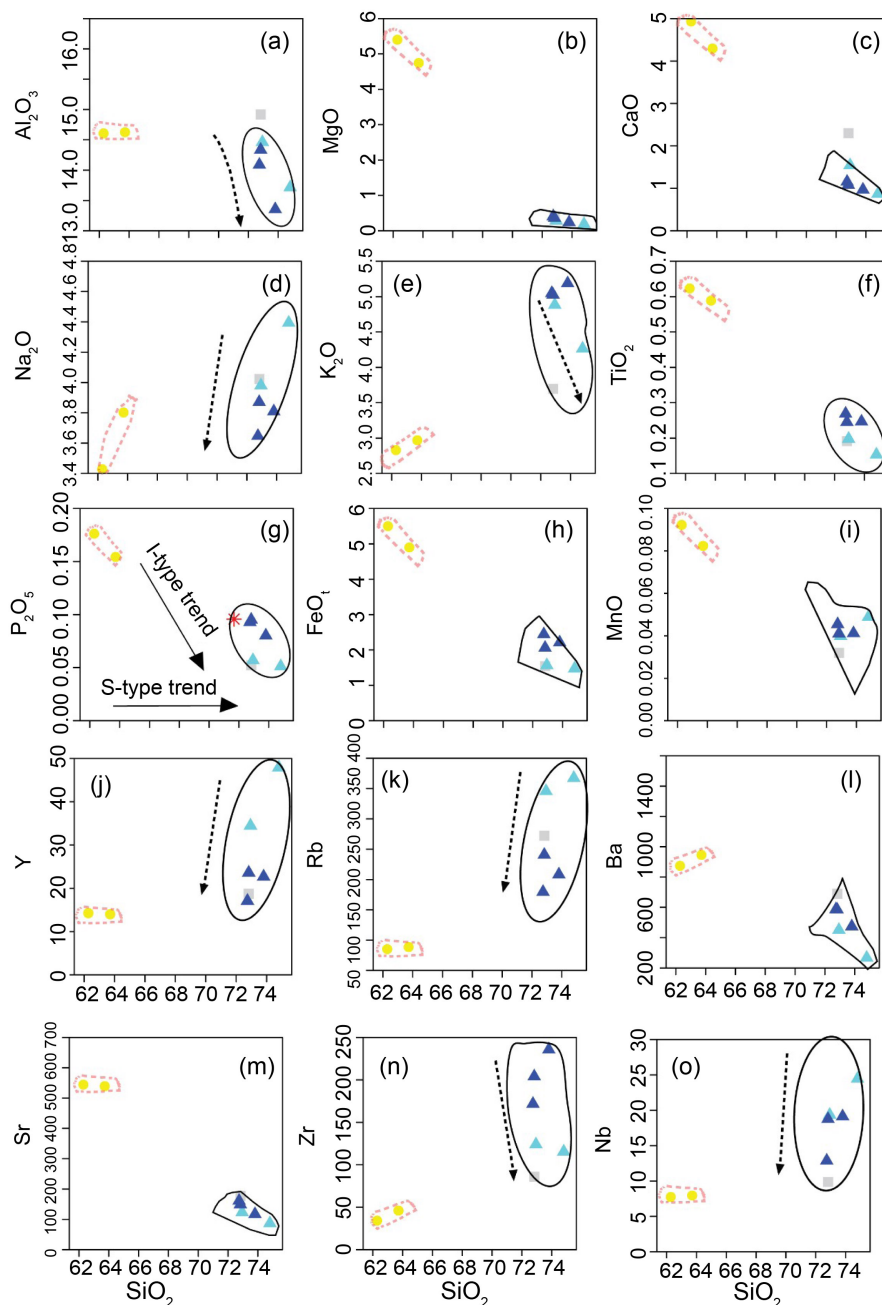


Figure 6. Variation of major and trace elements expressed as SiO_2 [23] of studied plutons.

defined by Barbarin [18]. The biotite and two-mica granites fall into the field of monzogranites, while the granodiorites fall into the field of quartz monzodiorites (Figure 7(a)). In the SiO_2 vs $\text{Na}_2\text{O} + \text{K}_2\text{O}$ classification diagram of [25], the plutons studied are subalkaline in nature, with compositions ranging from granodiorites to granites (Figure 7(b)); this is therefore consistent with the nomenclature of petrographic facies according to modal analyses. The expression of the aluminium saturation index ASI ($\text{Al}_2\text{O}_3/(\text{CaO} + \text{Na}_2\text{O} + \text{K}_2\text{O})$) as a function of SiO_2 [26] [27] [28] reveals the distinctly metaluminous character,

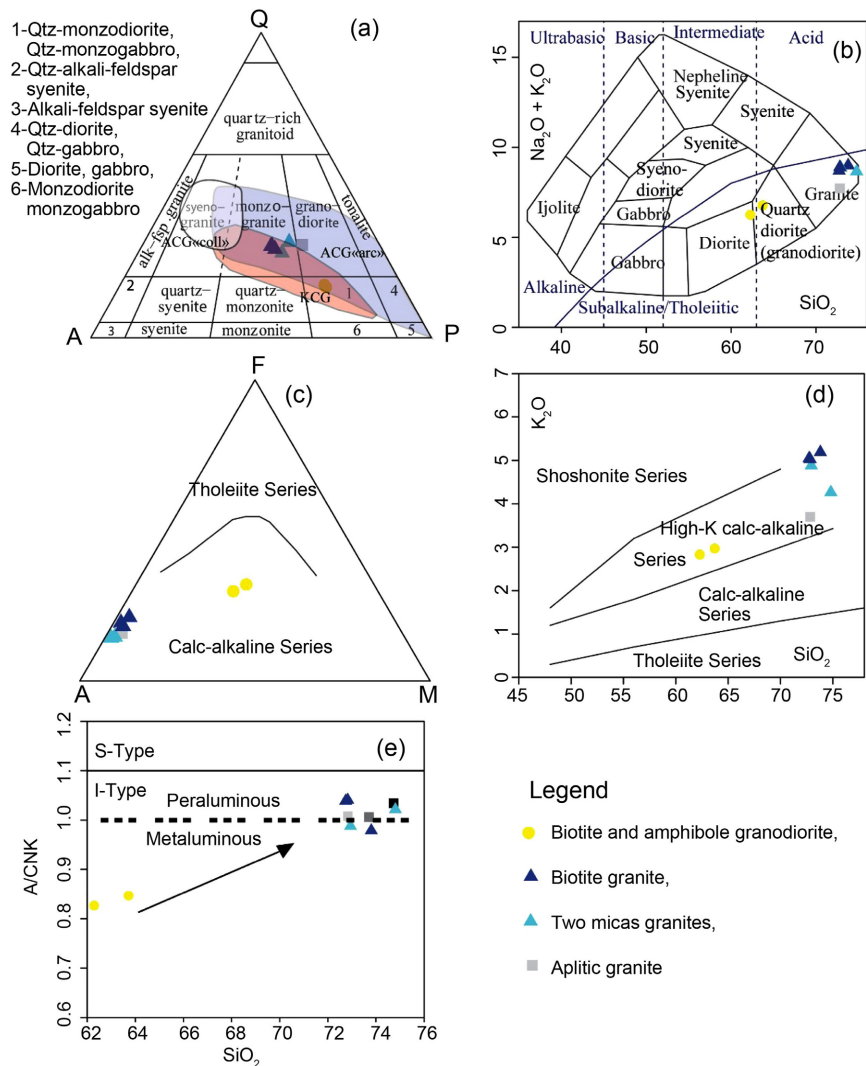


Figure 7. Chemical classification and nomenclature diagrams of Granitoids. (a) classification diagram Q (Quartz), A (Alkali feldspar), P (Plagioclases) from [24]; (b) SiO₂ vs Na₂O+K₂O diagram [25]; (c) AFM diagram (Na₂O + K₂O-MgO-Fe₂O₃) [29]; (d) K₂O vs SiO₂ diagram [30]; (e) expression of the aluminum saturation index ASI (Al₂O₃/(CaO + Na₂O + K₂O)) as a function of SiO₂ [26] [28].

with A/CNK ratios of less than unity ($0.83 \leq A/CNK \leq 0.85$) (Figure 7(e)) of the biotite and amphibole granodiorites compared with the biotite and two-mica facies whose samples straddle the metaluminous-peraluminous boundary with A/CNK ratios close to unity ($0.98 \leq A/CNK \leq 1.04$) (Figure 7(e)). All the plutons belong to the calc-alkaline series with a high potassium content, based on the AFM diagrams of [29] and K₂O vs SiO₂ of [30] (Figure 7(c) and Figure 7(d)).

4.2.2. Trace Elements

Compared to trace element concentrations ($267.54 \leq \text{Ba (ppm)} \leq 690.32$; $86.86 \leq \text{Sr (ppm)} \leq 177.53$; $7.89 \leq \text{Cr (ppm)} \leq 13.47$; $1.44 \leq \text{Co (ppm)} \leq 2.71$; $179.48 \leq \text{Rb (ppm)} \leq 367.49$ ppm; $9.88 \leq \text{Nb (ppm)} \leq 24.46$; $0.49 \leq \text{Ta (ppm)} \leq 1.69$;

$85.87 \leq \text{Zr (ppm)} \leq 235.75$; $17.09 \leq \text{Y (ppm)} \leq 47.91$; $15.04 \leq \text{Th (ppm)} \leq 29.75$) recorded in biotite and two-mica facies; biotite and amphibole granodiorites show high levels of the transition elements Ni (135.37 - 139.51 ppm), Cr (395.73 - 447.74 ppm), Co (19.22 - 20.47 ppm) and Large Ion Lithophile Elements (LILE) Ba (873.90 - 946.26 ppm) and Sr (539.35 - 544.37 ppm). Concentrations of High Field Strength Elements (HFSE) Y (13.97 - 14.25 ppm), Th (8.13 - 9.09 ppm), Nb (7.73 - 7.95 ppm), Ta (0.23 - 0.25 ppm), Hf (1.32 - 1.52 ppm), Zr (34.24 - 46.03 ppm) and LILE element Rb (179.48 - 367.49 ppm) remain moderate in these facies. The SiO_2 vs trace elements of the Harker diagram (**Figure 6**) shows a constant evolution of the elements Y, Rb, Sr and Nb in the biotite and amphibole granodiorites (**Figure 6(j)**, **Figure 6(k)**, **Figure 6(m)** and **Figure 6(o)**); incompatibility of the elements Zr, Th (not illustrated) and Ba (**Figure 6(l)**) and compatibility of the elements Cr (not illustrated), V (not illustrated), Co (not illustrated), Sc (not illustrated). In the two-mica and biotite granites, the elements Ba and Sr are compatible with a steeper negative slope for Ba (**Figure 6(l)** and **Figure 6(m)**), whereas the elements Th (not shown), Y, Rb, Zr and Nb (**Figure 6(j)**, **Figure 6(k)**, **Figure 6(n)** and **Figure 6(o)**) show steep falls for almost similar SiO_2 contents. The ORG-normalized multi-element diagrams [31] of the granitoids studied (**Figure 8**) are characterized by spectra enriched in LILE elements (K, Rb, Ba, Th) and LREE elements (Ce) relative to HFSE elements (Ta, Nb, Hf, Zr, Sm, Y, Yb). These spectra therefore show a decrease in the enrichment factor with increasing compatibility (**Figure 8(b)** and **Figure 8(d)**), which is similar to the spectra of granitoids from orogenic contexts [32]. These spectra also show a fall in Th to Ta and Nb and positive anomalies in Ce and Sm, characteristic of a strong crustal participation in the magmatogenesis of these rocks [31]. However, contrasts remain between the spectra of granodiorites and those of granites. Biotite and amphibole granodiorites show spectra enriched in the more incompatible elements (Rb, Ba and Th) while concentrations of Hf, Zr, Y and Yb remain low to very low. This is similar to the calc-alkaline granites of active continental margins and post-collision settings [31]. Biotite and the two-mica granites show spectra with negative Ba anomalies between the adjacent elements Rb and Th, reflecting the dominant control of alkali feldspars in the magmatic evolution of these rocks. Relative to the spectra of granodiorites, these facies show spectra that are more enriched in Nb, Ce, Hf, Zr and Sm, which is similar to the spectra of highly fractionated calc-alkaline granitoids (HFCA) emplaced in syn and post-collisional settings [31]. Rare Earth Elements (REE) contents are higher in biotite granites ($225.09 \leq \Sigma\text{REE} \leq 247.31$ ppm) compared to the two-mica granites ($83.40 \leq \Sigma\text{REE} \leq 139.45$ ppm) and biotite et amphibole granodiorites ($106.91 \leq \Sigma\text{REE} \leq 143.70$). The REE spectra normalized to chondrites [33] of the different petrographic entities are characterized by more fractionated profiles in Light Rare Earth Elements (LREE) ($3.02 \leq (\text{La/Sm}) \text{ N} \leq 6.33$) and relative to Heavy Rare Earth Elements HREE ($0.84 \leq (\text{Gd/Yb}) \text{ N} \leq 2.36$); this is characteristic of highly potassic rocks [34] [35]. However, contrasts appear

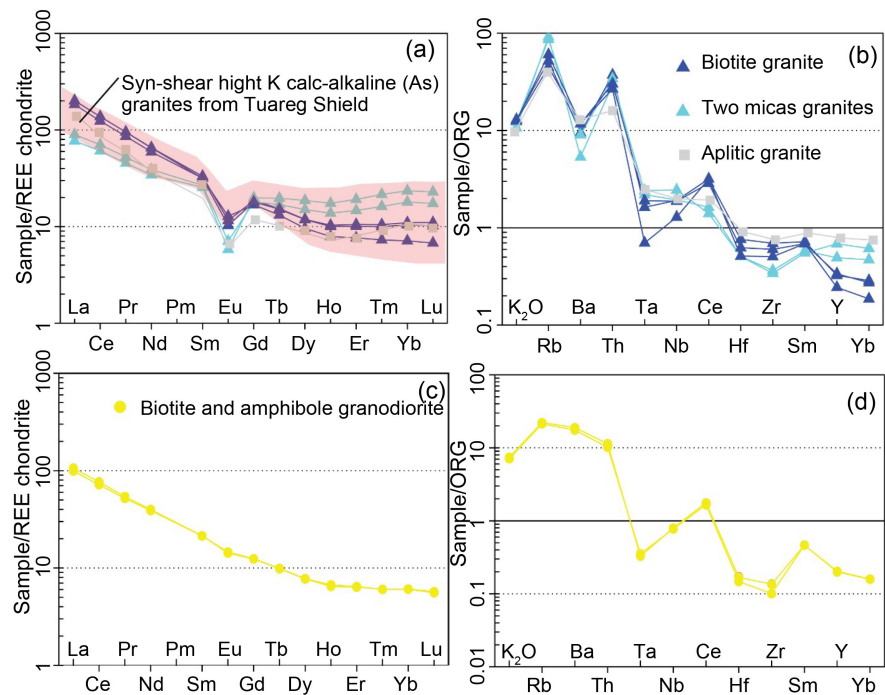


Figure 8. (a), (c) chondrite-normalized rare earth diagrams [33]; (b), (d) multi-elements diagrams normalized to ORG (oceanic ridge granite) [31].

between the different profiles. The biotite and amphibole granodiorites are characterized by highly fractionated profiles ($16.29 \leq (\text{La}/\text{Yb})_N \leq 17.53$) and a virtual absence of negative Eu anomalies ($0.87 \leq \text{Eu}^*/\text{Eu} \leq 0.90$), suggesting little involvement of plagioclases in their magmatic evolution. The high $(\text{La}/\text{Yb})_N$ ratios in these facies result from the depressed HREE character, giving these profiles an upward concavity. These types of profiles are indicative of the presence, among the melt residues, of a mineral phase that strongly fractionates the HREEs and corresponds to garnet and/or amphibole [36]. These spectra, marked by a regular slope from La to Lu with no negative Eu anomaly, are similar to granitoids from active continental margins [37]. Biotite and two-mica granites are distinguished from the previous facies by spectra with more pronounced Eu anomalies ($0.26 \leq \text{Eu}^*/\text{Eu} \leq 0.55$) reflecting the fractionation of plagioclases. However, there is a higher fractionation rate in biotite granites ($17.61 \leq (\text{La}/\text{Yb})_N \leq 28.13$) compared with the two-mica granites ($3.27 \leq (\text{La}/\text{Yb})_N \leq 6.29$), which rules out any genetic link between these two facies. However, the spectra of the two-mica granites remain closer to calc-alkaline granitoids than those of purely crustal leucogranites where the fractionation of HREE is very strong. The profiles of both two-mica and biotite granites are similar to those of high-potassium syn-shear granitoids of the Touareg Shield [38] (Figure 8(a)).

4.3. Zircon U-Pb Dating

To better define the geodynamic evolution of the granitoids associated with the Glito-Kpatala shear zone in south-east Togo, 2 representative samples of biotite

and two-mica granites were dated. The biotite and two-mica granite samples dated were sample 09A from the Adjako pluton and sample 10C from the Glito pluton. The results of the analyses carried out on these samples are reported in **Table 5**. The zircon grains in the dated samples show almost identical microscopic characteristics. They are automorphic to sub-automorphic, prismatic, often elongated or stocky, with a transparent to translucent lustre and a size of between 128 μm and 379 μm (**Figure 9(a)** and **Figure 9(b)**). Automorphous zircon crystals show regular concentric zoning with a bright luminescence suggesting a magmatic origin. Moreover, their Th/U ratios > 0.1 and between 0.24 and 1.181 are characteristic of magmatic zircons [39]. Eleven (11) and six (6)

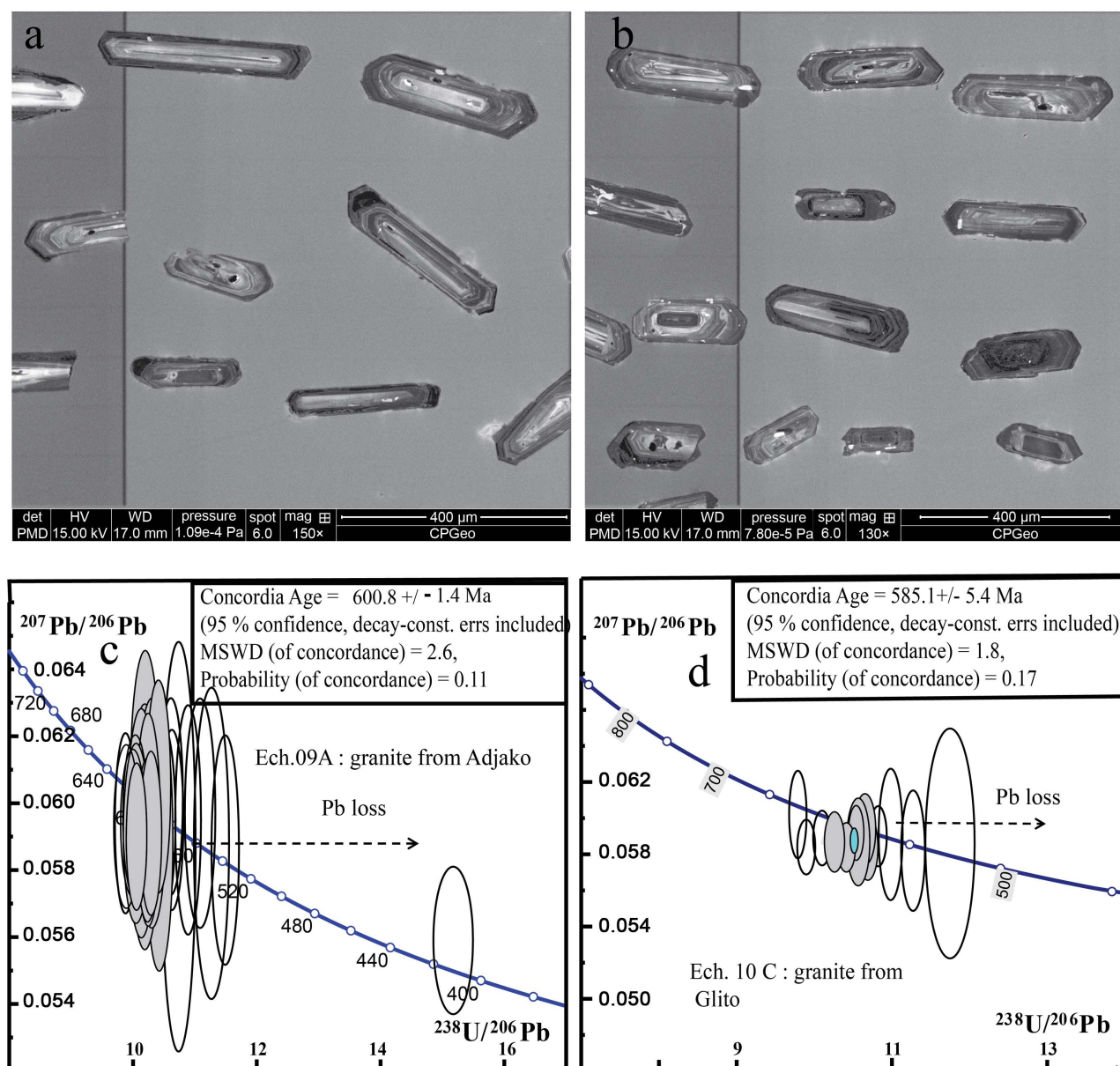


Figure 9. Cathodoluminescence images ((a), (b)) showing the representative textures of the zircon grains and Concordia diagram of the U-Pb ((c), (d)) results of the dated samples.

Table 5. Results of analysis of U-Pb dating on zircon of some granitoids from Southeastern Togo.

Spot	U (ppm)	Th (ppm)	Pb (ppm)	Th/U	207Pb/235U	1 σ	206Pb/238U	1 σ	238U/206Pb	1 σ	207Pb/206Pb	1 σ	208Pb/206Pb	1 σ
Sample 09A: Adjako Biotite Bearing granite														
1	281.4	114.1	36.6	0.406	0.778	0.0201	0.0959	0.0008	10.4325	0.0886	0.0589	0.0016	0.1738	0.0445
2	292.7	170.9	39.8	0.584	0.8011	0.0173	0.096	0.0007	10.4162	0.0809	0.0605	0.0013	0.1944	0.0182
3	500.5	131.3	62.7	0.262	0.7982	0.0189	0.097	0.0009	10.3099	0.0949	0.0597	0.0014	0.1074	0.0137
4	498.3	211.1	65	0.424	0.7912	0.0135	0.0971	0.0007	10.2943	0.0716	0.0591	0.001	0.1435	0.0112
5	415.2	190.2	52.5	0.458	0.8009	0.0175	0.0976	0.0008	10.2488	0.0792	0.0595	0.0013	0.1564	0.0061
6	351.5	192.6	50.9	0.548	0.7932	0.0135	0.0977	0.0007	10.2389	0.0713	0.0589	0.001	0.1677	0.0207
7	252.2	149.9	35.1	0.594	0.8161	0.0222	0.098	0.0009	10.2025	0.0981	0.0604	0.0017	0.2134	0.0457
8	417.2	311.1	57	0.746	0.802	0.0202	0.0981	0.0009	10.1947	0.0979	0.0593	0.0015	0.2177	0.026
9	426.4	196.2	52	0.46	0.8074	0.0192	0.0986	0.0009	10.1409	0.0937	0.0594	0.0014	0.1527	0.0069
10	716.6	271.8	94.4	0.379	0.8088	0.0124	0.0994	0.0007	10.065	0.0678	0.059	0.0009	0.115	0.0468
11	890	218.7	107.3	0.246	0.8103	0.0155	0.0994	0.0008	10.0569	0.0854	0.0591	0.0011	0.0944	0.0171
Sample 10C: Glito 2 micas bearing granite														
1	546.4	241.3	65.7	0.442	0.7526	0.0141	0.0935	0.0008	10.6948	0.086	0.0584	0.0012	0.1416	0.0027
2	447.2	281.1	56.6	0.628	0.7682	0.0158	0.0938	0.0008	10.6582	0.091	0.0594	0.0013	0.227	0.0187
3	326.1	185.9	41.8	0.57	0.7658	0.0187	0.0946	0.0009	10.5709	0.0985	0.0587	0.0016	0.2464	0.0427
4	878	360.5	106.1	0.411	0.7747	0.0127	0.0948	0.0006	10.5444	0.0654	0.0592	0.001	0.2219	0.0749
5	1182.4	483.2	138.6	0.409	0.7733	0.0118	0.096	0.0007	10.4192	0.0764	0.0584	0.0009	0.1275	0.0034
6	655.3	283.7	78.7	0.433	0.7883	0.0148	0.0974	0.0008	10.2652	0.0857	0.0587	0.0011	0.1051	0.0131

zircon grains from the biotite granite and two-mica granite respectively were analyzed (Table 5). There were wide variations in the U and Th contents of the zircons in the samples analyzed. The uranium and thorium contents in the zircon grains from the biotite granite sample vary between 252 and 890 ppm and between 114 and 311 ppm respectively, giving a Th/U ratio of between 0.246 and 0.746 and a Concordia age of 600.8 ± 1.4 Ma (MSWD = 2.6) (Figure 9(c)). In the two-mica granite sample, U and Th concentrations range from 326 - 1182 ppm and 185 - 483 ppm respectively. The six (06) analyses give a Concordia emplacement age of 585.1 ± 5.4 Ma (MSWD = 2.4) for Th/U ratios varying from 0.409 to 0.268 (Figure 9(d)).

5. Discussion

5.1. Main Magma Evolution Processes

Biotite and two-mica granites have distinct geochemical characteristics from biotite amphibole granodiorites. On the basis of linear relationships with the oxides MgO, FeO, MnO, CaO, TiO₂, P₂O₅, biotite and two-mica granites can be interpreted with certainty as granodiorite fractionation products. However, the variability of the oxides K₂O, Na₂O, Al₂O₃ (Figure 6) and the trace elements Y, Rb, Ba, Sr, Zr and Nb (Figure 8) in the Harker diagrams; the non-linear and dis-

tinct trends between granodiorites and granites in the Sr vs Ba, Sr vs Rb, La/Yb vs SiO₂, Dy/Yb vs SiO₂ and Sr/Y vs SiO₂ diagrams (Figure 10), rule out any origin of biotite and the two-mica granites by crystal fractionation from granodiorites. The correlations observed in the Harker diagrams highlight differences in magmatic evolution. In the granodiorites, the systematic decrease in Ti, Al, Fe, Mg, Ca and Mn oxides with increasing acidity is compatible with the fractionation of ferromagnesian, in particular amphibole, sphene and calcic plagioclases. The trend towards enrichment in K₂O and Na₂O and the weak negative to positive correlation shown by the Ba and Sr with increasing acidity,

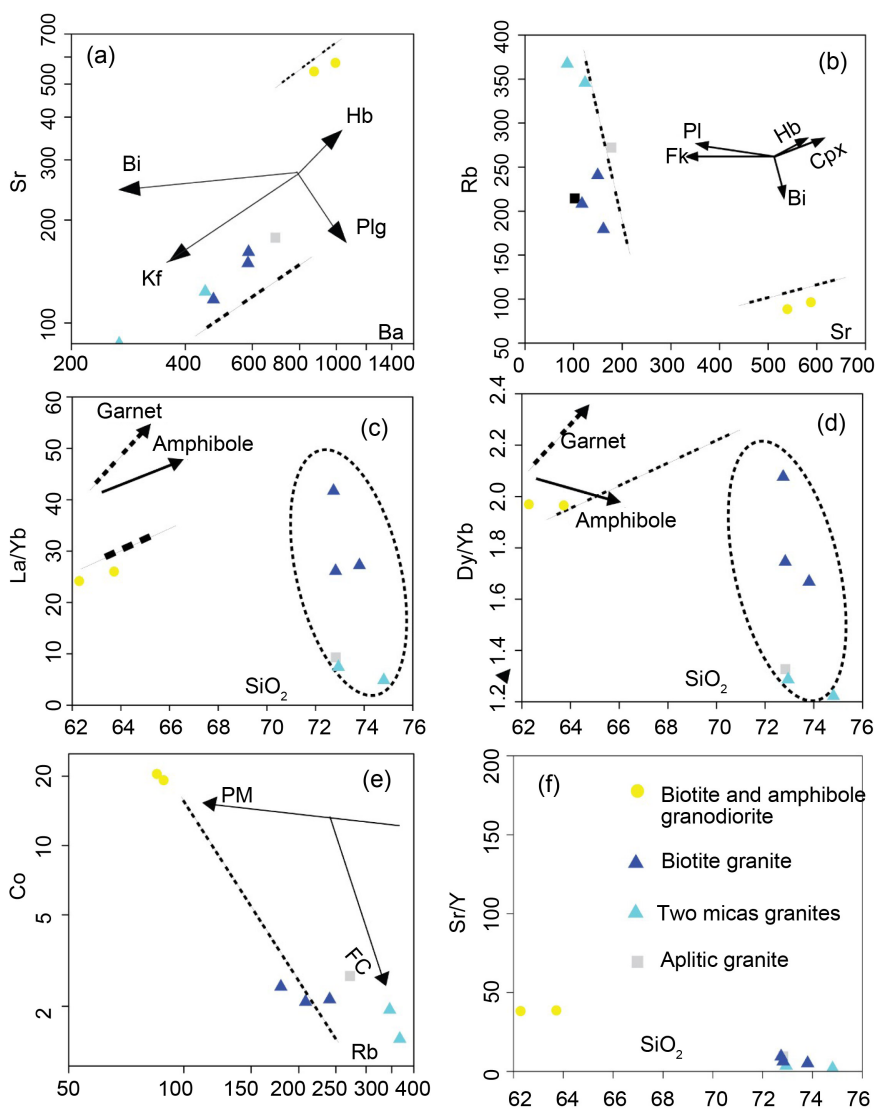


Figure 10. Diagrams of binary log Sr vs Log Ba (a), Rb vs Sr (b) plots of the studied plutons. Mineral vectors are computed according to [47] partition coefficient; variation diagrams La/Yb vs. SiO₂ (c) Dy/Yb vs SiO₂ (d). The fractional crystallization (FC) vectors of garnet and amphibole in (c) and (d) are derived from [48] [49]; (e) Classification diagram of compatibles elements log(Co) versus incompatible elements log(Rb) [50] indicating that fractional crystallization (FC) rather than partial melting (PM) dominated the genesis of the studied plutons; (f) binary diagram Sr/Y vs. SiO₂ according to [51].

reflects the virtual absence or very low involvement of alkali feldspars in the differentiation process of these rocks. This is supported by the absence of a negative Ba anomaly and the low negative Eu anomaly in the ORG-normalized multi-element diagrams (**Figure 9(b)** and **Figure 9(d)**) and the chondrite-normalized rare earth spectra (**Figure 8(a)** and **Figure 8(c)**) respectively. In biotite and two-mica granites, the inflections in Na_2O and Al_2O_3 and K_2O , the relative depletion in CaO, Sr and Ba and the negative anomalies in Eu indicate the fractionation of alkali feldspars. Slight decreases in MgO, TiO_2 , FeO, MnO and P_2O_5 are consistent with fractionation of biotite, muscovite (in two-mica facies) and apatite. The fractional crystallization processes occurring during the evolution of a granitic magma can be reflected through correlations in Sr, Ba and Rb trace element binary diagrams [40]. The Sr vs Rb and Sr vs Ba diagrams (**Figure 10(a)** and **Figure 10(b)**), which clearly and unambiguously distinguish essentially two populations of points, show on the one hand the predominant role of potassic feldspars and biotite in the evolution of biotite and two-mica granites and on the other hand a magmatic differentiation process controlled mainly by the fractionation of amphiboles in biotite amphibole granodiorites. It therefore seems that the fractionation of amphiboles and the partial differentiation of LREEs from HREEs linked to garnet retention at the source, controlled the upward concave shape of the REE spectra of granodiorites [41] [42] [43]. This hypothesis is also confirmed by the increase in La/Yb and Dy/Yb ratios with increasing acidity (**Figure 10(c)** and **Figure 10(d)**). In the classification diagram of compatible (Co) versus incompatible (Rb) elements, the samples mainly show a downward trend in compatible versus incompatible elements (**Figure 10(e)**), reflecting the role of fractional crystallization as the main evolutionary process in the plutons studied. In biotite and amphibole facies, the low Rb content and high Ba and Sr contents, combined with the near absence of Eu negative anomalies (**Figure 8(c)**) suggest that these facies are not very evolved and that fractional crystallization of feldspars and biotite was not an important process [44]. Compared with granodiorites, biotite and two-mica granites have higher SiO_2 contents and much lower concentrations of TiO_2 , MgO, FeO and CaO (**Figure 7**). These rocks are also enriched in Rb, Th and U and show marked depletions in Ba, Sr, Ti and Eu, which suggests that they have undergone greater fractionation [45] [46] and are therefore more evolved.

5.2. Geochemical Signature and Petrogenesis

Several mineralogical and geochemical characteristics of the plutons studied are consistent with I type calc-alkaline granitoids. These characteristics include: 1) their metaluminous to weakly peraluminous nature with an ASI ratio ≤ 1.1 (**Figure 7(e)**) [27], 2) the presence of modal amphibole and accessory sphene in the biotite and amphibole facies [18], 3) all the samples studied show a marked decrease in P_2O_5 oxide with the increase in SiO_2 (**Figure 6**). This attribute is a key criterion for distinguishing type I granites from type S granites [26]. More

precisely, biotite and amphibole granodiorites are similar to ACG granitoids (Amphibole-rich Calc-alkaline Granitoids) while biotite and two-mica granites are comparable to KCG granitoids (K-rich and K-feldspar porphyritic Calc-alkaline Granitoids) if we stick to the Barbarin (1999) terminology [18] (Figure 7(a)). According to the latter, both ACG and KCG granitoids result from interactions between basaltic magma derived from the mantle and crustal rocks melted in variable proportions. The Th/Ta ratio is an important marker of mantle-crust interaction since mantle-derived rocks are expected to have Th/Ta ratios close to 2, lower than those of the lower continental crust (Th/Ta = 7.9) and upper continental crust (Th/Ta = 6.9) [52]. The Th/Ta ratios of the samples studied vary considerably between 14.04 and 43.82, with an average of 26.05 (Table 2), indicating a strong involvement of a crustal source rock in the formation process of these rocks. This is borne out by the Zr/Hf (25.27 to 37.21, average = 30.67 ppm), Th/U (2.58 to 15.05 ppm, average = 5.85 ppm) and Rb/Sr (0.16 to 4.32; mean = 1.67 ppm) from these rocks, which are fairly close to the crustal values defined by some authors ($31 \leq \text{Zr/Hf} \leq 36$; $3.8 \leq \text{Th/U} \leq 5.9$; $0.18 \leq \text{Rb/Sr} \leq 0.32$) [53]-[59]. Experimental data on calc-alkaline granitoids with high K contents, such as the plutons studied, show that these rocks can be produced by the melting of different crustal sources [60]. In addition, the partial melting of common crustal rocks, such as amphibolites, tonalitic gneisses, metagreywackes and metapelites, under variable melting conditions, produces compositional differences between magmas [61]. The biotite amphibole granodiorites are characterised by high CaO/Na₂O ratios (0.47 - 1.44 ppm) and moderate Rb/Sr (0.14 - 0.27 ppm) and Rb/Ba (0.07 - 0.14 ppm) ratios, reflecting a source rich in plagioclase and therefore not metapelite [54] [62]. These facies, which are almost devoid of negative Eu anomalies, show strongly fractionated REE spectra (Figure 9(c)), very high content of transition elements Ni (135.37 - 139.51 ppm) and Cr (395.73 - 447.74 ppm) and high Sr/Y ratios (38.21 - 174.42 ppm) suggesting their origin from a mafic to intermediate lower continental crust where garnet and/or amphibole were stable residual assemblage minerals (e.g., garnet amphibolites or amphibole eclogite [37] [63]. Studies [64] have shown that such magmas with a high K content ($2.83 \leq \text{K}_2\text{O} \leq 4.15$, $62.29 \leq \text{SiO}_2 \leq 70.28$) can only be obtained by the partial melting of hydrated mafic metamorphic rocks (amphibolites) that are calc-alkaline and have a high K content. This hypothesis is supported by the experimental binary diagram Al₂O₃ + FeOt + MgO + TiO₂ vs. Al₂O₃/(FeOt + MgO + TiO₂) from [51] where the samples representative of biotite and amphibole facies are clearly in the range of rocks derived from the melting of amphibolite (Figure 11(a)). The moderate CaO/Na₂O ratios (0.20 - 0.57 ppm, mean = 0.38 ppm), low Rb/Ba ratios (0.39 - 1.37, mean = 0.84 ppm) and fairly varied Rb/Sr ratios (1.53 - 4.23 ppm, mean = 2.85 ppm) in the two-mica granites indicate their predominant derivation from psammitic and pelitic metasediments rather than metagreywackes, while these low ratios ($0.25 \leq \text{CaO/Na}_2\text{O} \leq 0.32$, mean = 0.28 ppm; $0.31 \leq \text{Rb/Ba} \leq 0.44$, mean = 0.39 ppm; $1.11 \leq \text{Rb/Sr} \leq 1.78$, mean = 0.39

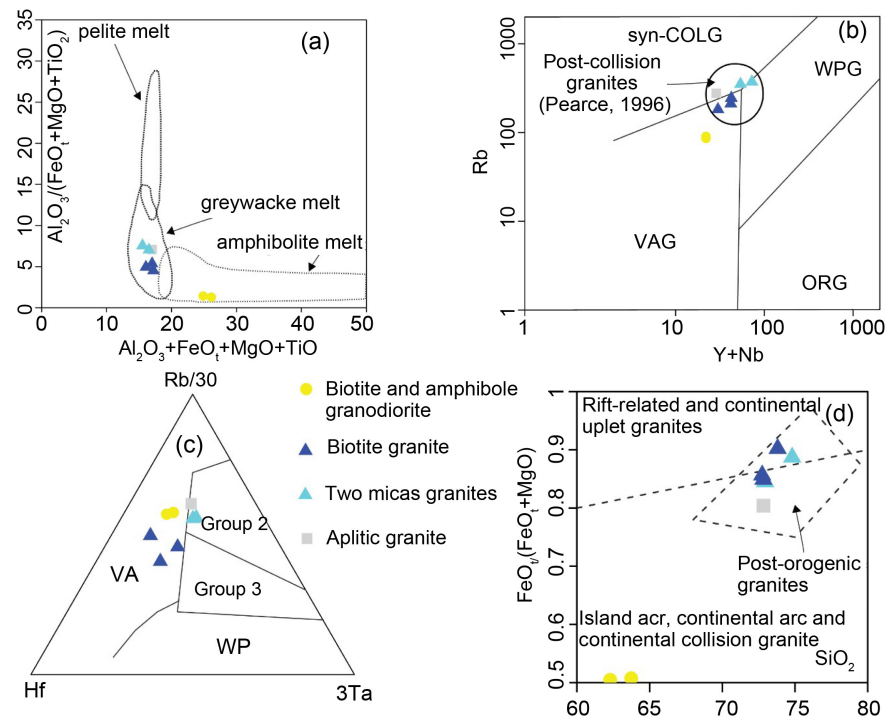


Figure 11. (a) Binary graphic of $(\text{Al}_2\text{O}_3 + \text{FeO} + \text{MgO} + \text{TiO}_2)$ vs. $(\text{Al}_2\text{O}_3/(\text{FeO} + \text{MgO} + \text{TiO}_2))$ from [51]; (b) geotectonic discrimination diagrams $Y + \text{Nb}$ vs. Rb [70]. WPG: Intra-plate granites, ORG: Oceanic ridge granites; VAG: volcanic arc granites; Syn-COLG: Syn-collisional granites; (c) Rb-Ta-Hf discrimination diagram [72]. Group 2: Syncollisional; Group 3: tardi and post-collisional, VA: volcanic arcs, WP: intraplate; d- SiO_2 vs. $\text{FeO}^*/(\text{FeO}^* + \text{MgO})$ [71].

ppm) in biotite granites are more consistent with melting from a metagreywackes source [51] [54] [62]. This is in line with the negative Eu and Ba anomalies and the Sr depletion that would be favoured by anatexis of a feldspar-rich source, leaving a large proportion of this mineral in the residue [62] [65]. The moderate Sr/Y ratios (1.81 - 9.47 ppm) and the low levels of transition elements Ni (1 - 6.44 ppm) and Cr (7.89 - 13.47 ppm) in both the two-mica and biotite granites are consistent with their emplacement at relatively shallow depths in the upper to mean continental crust, under pressures of less than 10 Kbar [37] [63]. The presence of dioritic magmatic enclaves both in biotite and amphibole facies and in two-mica facies suggests a mixture of externally injected mafic magma and granitic host magmas. This hypothesis is supported by the predominantly rounded or ovoid shape of the enclaves and their frozen edges, reflecting the rheological difference between the two magmas of contrasting compositions, which solidified at different times [66]. The presence of micrograined magmatic enclaves of a dioritic nature is commonly cited as evidence of interaction between a mantle-derived mafic magma and a granitic magma [60]. However, the lack of geochemical data (radiometric isotopes, major and trace elements) on the enclaves rules out any speculative inference about their mantle origin. The Nb/Ta ratios in biotite and amphibole facies (31.25 - 34.61 ppm) and even in some bio-

tite facies (14.14 - 26.36 ppm) that are fairly close to mantle estimates than crustal averages would be geochemical markers of a probable intervention of a mantle source in the genesis of these rocks. Indeed, primitive mantle and mantle-derived molten rocks generally have high Nb/Ta ratios (>17.5) [65] [67] relative to typical continental crust, which is estimated to be much lower (11 - 13 ppm) [57] [58] [59] [68].

5.3. Geodynamic Context of Emplacement

The Large Ion Lithophile Elements (LILE) and High Field Strength Elements (HFSE) contents of granitoids varies according to the source and the tectonic context in which the granitoids were emplaced during an orogeny [69]. In fact, such discrimination often proves inconclusive, particularly for magmas derived from complex processes (multiple sources, mixtures, more or less complex crustal contamination processes). Similarly, post-collision granitoids are difficult to differentiate from certain volcanic arc and intraplate granitoids [69]. In the Rb vs (Nb + Y) [70] and SiO_2 vs $\text{FeO}^*/(\text{FeO}^* + \text{MgO})$ [71] diagrams (**Figure 11(b)** and **Figure 11(d)**), the biotite and amphibole granodiorite samples show that they belong strongly to the arc granitoids (volcanic, continental) whereas the biotite and two-mica granite samples are spread out in the field of postcollisional granitoids. In the Rb-Ta-Hf diagram [72], the granodiorites and biotite granites are positioned in the volcanic arc granitoid domain while the two-mica granites fall slightly into the syncollisional granitoid space (**Figure 11(c)**). The syncollisional context of the two-mica granites can most probably be excluded due to the high-potassium calc-alkaline nature of these rocks. These geotectonic discrimination diagrams therefore suggest that the plutons studied were emplaced in two distinct geodynamic settings, *i.e.* in a post-collisional setting and in an arc setting overlying subduction. The recent ages of 600 ± 1.4 Ma and 585 ± 5.4 Ma obtained for the biotite and two-mica granites respectively are inconsistent with arc magmatism overriding subduction in view of the model for the evolution of the Pan-African Dahomeyides chain marked by a collision around 610 Ma [73] and the operation of post-collisional ductile unconformity from 606 Ma [8]. The ages and the great similarity of the REE profiles of the biotite and two-mica granites with those of the postcollisional calc-alkaline Pan-African granites with a high K content of the Air massif of the Touareg shield [38] (**Figure 8(a)**) remove any doubt as to the emplacement of the biotite and two-mica granites in a post-collisional context. The lack of radiometric data on biotite and amphibole granodiorites still maintains doubt as to their emplacement in a post-collisional context. However, certain petrographic (presence of biotite and amphibole) and geochemical characteristics ($\text{TiO}_2 < 0.87\%$, enrichment in K, Ba, Th and LREE; Rb/Zr ratio close to 2 with an average of 2.2) assimilate them to the post-collisional granites [72] and of the Mlo (Mixed, late-orogenic) type [74]. The arc geochemical signatures, also observed in studies of Caledonian post to late collisional granites [75], would be inherited either from a component from the mantle that

was associated with a subduction zone [72] or from a crust that acquired this orogenic character during an earlier subduction. This hypothesis is quite plausible because the vestiges of subduction in this zone of the Pan-African Dahomeyides chain are the eclogites of the Lato Mountains [12] [76] and the arc base granulites of the Agou and Kabyè Mountains [77]. The emplacement of these post-collisional granitoids in an intracontinental environment close to a shear zone [78] makes it possible to envisage the “adiabatic decompression” model [79]. In fact, the generation and ascent of a basic and independent magma, a heat carrier, will cause the lower continental crust to melt [80] [81]. In view of the geochemical and geochronological data obtained on the granites studied and the similarity with the spectral profiles of the calc-alkaline granitoids with a high potassium content from the Tuareg shields (Figure 8(a)), the granitoids studied can be integrated into the pan-African late magmatic episode of the Dahomeyides, which corresponds between 606 and 583 Ma [8], to the activity of transcurrent ductile strike-slips and to the synchronous emplacement of calc-alkaline plutons with a high potassium content in a post-collisional context. These high-K calc-alkaline magmatic episodes K (HKCA) are well known in many segments of the Pan-African chain, particularly in Benin in the major shear zone at Kandi (central Benin) where work carried out [8], highlighted the existence of a shear-synchronous magmatic episode marked by the emplacement of calc-alkaline granitoids with a high potassium content at Tchetti (607 ± 11 Ma), Gobada (603 ± 10 Ma), Tré (595 ± 12 Ma) and Fita (594 ± 32 Ma). This post-collisional magmatic episode is preceded at the sub-regional scale by the tectono-metamorphic event associated with the collision, the peak of which is in the granulite facies dated at 610 ± 2 Ma by [82] and at 612.5 ± 0.8 Ma by [73].

6. Conclusions

The granitoids associated with the Glito-Kpatala shear zone, emplaced around 592 Ma, are among the igneous plutonic assemblages that have marked Pan-African late-orogenic history. As petrographic studies indicate, these plutons, which outcrop in the inner zone of the Pan-African Dahomeyid chain, are composed of four facies: biotite-amphibole granodiorites, biotite granites, two-mica granites and aplitic granites, which are very poorly represented.

- The biotite and amphibole granodiorites have a mineralogy essentially of plagioclase of the andesine to oligoclase type (An₁₆₋₄₃), quartz, calcic amphibole of the magnesiohornblende to actinote type, potassic feldspar and magnesian biotite of the phlogopite type. Apart from muscovite, which appears in two-mica facies, biotite and two-mica granites share a common mineralogical composition consisting mainly of quartz, potassium feldspar, plagioclase of albite to oligoclase type and annite-type ferriferous biotite.
- The chemical and mineralogical compositions of the different facies indicate that these rocks are I type and belong to the high K calc-alkaline series, with a purely metaluminous chemical character displayed by the biotite and am-

phibole granodiorites compared with the biotite and two-mica facies whose chemical compositions vary between metaluminous and peraluminous. More precisely, the mineralogy of the plagioclases and the chemical composition of the plutons studied show, in Barbarin's terminology [18], that biotite and amphibole granodiorites are similar to ACG granitoids (amphibole-rich calc-alkaline granitoids) and biotite and two-mica granites are comparable to KCG granitoids (K-rich and K-feldspar porphyritic calc-alkaline granitoids).

- The magmatic evolution of biotite and amphibole granodiorites is distinguished from other facies by the enrichment of K_2O , Na_2O oxides and the element Ba; a constant progression of Sr and the absence of a negative Eu anomaly reflecting an evolutionary trend dominated by amphibole fractionation. As for the biotite and two-mica granites, their evolution marked the inflections in the oxides Na_2O , Al_2O_3 and K_2O , the relative depletion of Sr and Ba and the negative anomalies in Eu indicate a magmatic evolution dominated by alkali feldspars and biotite to a lesser extent.
- The values of the Th/Ta, Th/U, Zr/Hf and Rb/Sr ratios of the granitoids studied reveal a strong involvement of crustal source in the magmatogenesis of these rocks. Variations in the CaO/ Na_2O (0.47 - 1.44 ppm), Rb/Sr (0.14 - 0.27 ppm), Rb/Ba (0.07 - 0.14 ppm) and Sr/Y (38.21 - 174.42 ppm) ratios show that the biotite and amphibole granodiorites with their excessive Ni (135.37 - 139.51 ppm) and Cr (395.73 - 447.74 ppm) contents derive from a mafic to intermediate lower continental crust where garnet and/or amphibole were stable residual assemblage minerals. The moderate Sr/Y ratios (1.81 - 9.47 ppm) and low transition elements Ni (1 - 6.44 ppm) and Cr (7.89 - 13.47 ppm) contents in both the two-mica and biotite granites are consistent with their emplacement at relatively shallow depths in the mean to upper continental crust, at pressures below 10 Kbar. The moderate CaO/ Na_2O (0.20 - 0.57 ppm, mean = 0.38 ppm), low Rb/Ba (0.39 - 1.37, mean = 0.84 ppm) and fairly varied Rb/Sr (1.53 - 4.23 ppm, mean = 2.85 ppm) in the two-mica granites indicate their predominant derivation from psammitic and pelitic metasediments rather than metagreywackes, while these low ratios ($0.25 \leq CaO/Na_2O \leq 0.32$, mean = 0.28 ppm; $0.31 \leq Rb/Ba \leq 0.44$, mean = 0.39 ppm; $1.11 \leq Rb/Sr \leq 1.78$, mean = 0.39 ppm) in biotite granites are more consistent with melting from a metagreywacke-derived source. Evidence for the contribution of mantle-derived mafic magma with granitic magma in the plutons studied is materialized by the presence of magmatic enclaves in both granodiorites and two-mica granites, the volcanic arc geochemical signatures displayed by the plutons in geotectonic diagrams and Nb/Ta ratios (14.14 - 34.61 ppm) closer to mantle estimates.
- Geochemical data and radiometric dating elements suggest that the granitoids studied can be integrated into the pan-African late magmatic episode, which corresponds between 606 and 583 Ma [8], to the activity of transcurrent ductile strike-slips and to the synchronous emplacement of high K

calc-alkaline plutons in a post-collisional context.

Conflicts of Interest

The authors declare no conflicts of interest regarding the publication of this paper.

References

- [1] Kpanzou, S.A.M., Agbossoumondé, Y., González-Jiménez, J.M., Tairou, M.S. and Garcia-Casco, A. (2022) Pétrologie et métallogénie des indices de Ni-Cr associés au massif basique-ultrabasique de Oké, Togo. *Afrique SCIENCE*, **21**, 53-69. <https://www.afriquescience.net/PDF/21/1/5.pdf>
- [2] Ganade de Araujo, C.E., Cordani, U.G., Agbossoumondé, Y., Caby, R., Basei, M.A.S., Weinberg, R.F. and Sato, K. (2016) Tightening-Up NE Brazil and NW Africa Connections: Advances in Zircon Geochronology towards a Complete Plate Tectonic Cycle in the Dahomeyide Belt of the West Gondwana Orogen in Togo and Benin. *Precambrian Research*, **276**, 24-42. <https://doi.org/10.1016/j.precamres.2016.01.032>
- [3] Caen-Vachette, M., Pinto, M. and Roques, K.J.M. (1979) Plutons éburnéens et métamorphisme dans le socle cristallin de la chaîne pan-africaine au Togo et au Bénin. *Revue de Géologie Dynamique et de Géographie Physique*, **21**, 351-357.
- [4] Kalsbeek, F., Affaton, P., Ekwueme, B., Frei, R. and Thrane, K. (2012) Geochronology of Granitoid and Metasedimentary Rocks from Togo and Benin, West Africa: Comparisons with NE Brazil. *Precambrian Research*, **196/197**, 218-233. <https://doi.org/10.1016/j.precamres.2011.12.006>
- [5] Ferré, E., Gleizes, G. and Caby, R. (2002) Obliquely Convergent Tectonics and Granite Emplacement in the Trans-Saharan Belt of Eastern Nigeria: A Synthesis. *Precambrian Research*, **114**, 199-219. [https://doi.org/10.1016/S0301-9268\(01\)00226-1](https://doi.org/10.1016/S0301-9268(01)00226-1)
- [6] Rahaman, M.A., van Breemen, O., Bowden, P. and Bennett, J.N. (1984) Age Migrations of Anorogenic Ring Complexes in Northern Nigeria. *The Journal of Geology*, **92**, 173-184. <https://doi.org/10.1086/628847>
- [7] Castaing, C., Aregba, A. and Chevremont, P. (1988) Les unités gneissiques et la zone de cisaillement crustal du Sud-Togo (Gneissic Units and Crustal Shear Zone of South Togo). *Journal of African Earth Sciences*, **7**, 821-828.
- [8] Adissin Glodji, C. L. (2012) La zone de cisaillement de Kandi et le magmatisme associé dans la région de Savalou-Dassa (Bénin): Étude structurale, pétrologique et géochronologique. *Sci. de la Terre*, 276 p.
- [9] Affaton, P. (1990) Le bassin des Volta (Afrique de l'Ouest): Une marge passive d'âge protérozoïque supérieur, tectonisée au Panafricain (600±50 Ma). Edit. ORSTOM, Collection Etudes & Thèses, Paris, 500 p.
- [10] Agbossoumondé, Y., Ménot, R.-P., Paquette, J.L., Guillot, S., Yéssoufou, S. and Perache, C. (2007) Petrological and Geochronological Constraints on the Origin of the Palimé-Amlamé Granitoids (South Togo, West Africa): A Segment of the West African Craton Paleoproterozoic Margin Reactivated during the Pan-African Collision. *Gondwana Research*, **12**, 476-488. <https://doi.org/10.1016/j.gr.2007.01.004>
- [11] Attoh, K. and Morgan, J. (2004) Geochemistry of High-Pressure Granulites from the Pan-African Dahomeyide Orogen, West Africa: Constraints on the Origin and Composition of Lower Crust. *Journal of African Earth Sciences*, **39**, 201-208 <https://doi.org/10.1016/j.jafrearsci.2004.07.048>

- [12] Ménot, R.-P. and Seddoh, K.F. (1985) The Eclogites of Lato Hills (South Togo, West Africa): Relics from Early Tectonometamorphic Evolution of the Pan-African Orogeny. *Chemical Geology*, **50**, 313-330. [https://doi.org/10.1016/0009-2541\(85\)90126-3](https://doi.org/10.1016/0009-2541(85)90126-3)
- [13] Attoh, K. (1998a) High-Pressure Granulite Facies Metamorphism in the Pan-African Dahomeyide Orogen, West Africa. *The Journal of Geology*, **106**, 236-246. <https://doi.org/10.1086/516019>
- [14] Caby, R. and Boessé, J.M. (2001) Pan-African Nappe System in Southwest Nigeria: The Ife-Ilesha Schist Belt. *Journal of African Earth Sciences*, **33**, 211-225. [https://doi.org/10.1016/S0899-5362\(01\)80060-9](https://doi.org/10.1016/S0899-5362(01)80060-9)
- [15] Glodji, L.A., Komadja, C. and Yessoufou, S. (2017) Mise en place de magmas anté et syn-tectonique dans le complexe intrusif de Wari-Marou dans la zone de cisaillement de Kandi, Centre-Bénin, Afrique de l'Ouest. *Afrique SCIENCE*, **13**, 202-211. <http://www.afriquescience.info>
- [16] Ludwig, K.R. (2006) User's Manual for Isoplot 3.00: A Geochronological Toolkit for Microsoft Excel. <https://worldcat.org/title/695595118>
- [17] Didier, J. (1974) Granites and Their Enclaves. The Bearing of Enclaves on the Origin of Granites. *Geological Magazine*, **111**, 467-468.
- [18] Barbarin, B. (1999) A Review of the Relationships between Granitoid Types, Their Origins and Their Geodynamic Environments. *Lithos*, **46**, 605-626. [https://doi.org/10.1016/S0024-4937\(98\)00085-1](https://doi.org/10.1016/S0024-4937(98)00085-1)
- [19] Dada, O.A. (2012) Geochemistry of Biotite and Its Implications to the Origin of Bauchi and Saminaka Charnockites, North Central Nigeria. *International Journal of Geology, Earth & Environmental Sciences*, **2**, 163-172.
- [20] Abdel-Rahman, A.F.M. (1994) Nature of Biotites from Alkaline, Calc-Alkaline, and Peraluminous Magmas. *Journal of Petrology*, **35**, 525-541. <https://doi.org/10.1093/petrology/35.2.525>
- [21] Leake, B.E. (1997) Nomenclature of Amphiboles: Report of the Subcommittee on Amphiboles of the International Mineralogical Association, Commission on New Minerals and Mineral Names. *The Canadian Mineralogist*, **35**, 219-246.
- [22] Miller, C.F., Stoddard, E.F., Bradfish, L.J. and Dollase, W.A. (1981) Implications Composition of Plutonic Muscovite. *The Canadian Mineralogist*, **19**, 25-34. https://rruff.geo.arizona.edu/doclib/cm/vol19/CM19_25.pdf
- [23] Harker, A. (1909) *The Natural History of Igneous Rocks*. Methuen and Co., London, 420-423. <https://doi.org/10.1017/s0016756800124744>
- [24] Streckeisen, A. (1974) Classification and Nomenclature of Plutonic Rocks Recommendations. *Neues Jahrbuch für Mineralogie, Monatshefte*, **1973**, 149-164. <https://doi.org/10.1127/njmm/1973/1973/149>
- [25] Cox, K.G., Bell, J.D. and Pankhurst, R.J. (1979) *The Interpretation of Igneous Rocks*. George Allen & Unwin, London, 450 p. <https://doi.org/10.1007/978-94-017-3373-1>
- [26] Chappell, B.W. (1999) Aluminium Saturation in I- and S-Type Granites and the Characterization of Fractionated Haplogranites. *Lithos*, **46**, 535-551. [https://doi.org/10.1016/S0024-4937\(98\)00086-3](https://doi.org/10.1016/S0024-4937(98)00086-3)
- [27] Chappell, B.W., Bryant, C.J. and Wyborn, D. (2012) Peraluminous I-Type Granites. *Lithos*, **153**, 142-153. <https://doi.org/10.1016/j.lithos.2012.07.008>
- [28] Abdel-Rahman, A.F.M. (2017) Low- and High-Temperature Granites. *Lithos*, **27**, 177-193. <https://doi.org/10.1016/j.lithos.2012.07.008>

- [29] Irvine, T.N. and Baragar, W.R.A. (1971) A Guide to the Chemical Classification of the Common Volcanic Rocks. *The Canadian Journal of Earth Sciences*, **8**, 523-548. <https://doi.org/10.1139/e71-055>
- [30] Peccerillo, A. and Taylor, S.R. (1976) Geochemistry of Eocene Calc-Alkaline Volcanic Rocks from the Kastamonu Area, Northern Turkey. *Contributions to Mineralogy and Petrology*, **58**, 63-81. <https://doi.org/10.1007/BF00384745>
- [31] Pearce, J.A., Harris, N.B.W. and Tindle, A.G. (1984) Trace Element Discrimination Diagrams for the Tectonic Interpretation of Granitic Rocks. *Journal of Petrology*, **25**, 956-983. <https://doi.org/10.1093/petrology/25.4.956>
- [32] Frost, B.R., Barnes, C.G., Collins, W.J., Arculus, R.J., Ellis, D.J. and Frost, C.D. (2001) A Geochemical Classification for Granitic Rocks. *Journal of Petrology*, **42**, 2033-2048. <https://doi.org/10.1093/petrology/42.11.2033>
- [33] Boynton, W.V. (1984) Cosmochemistry of the Rare Earth Elements: Meteorite Studies. In: *Developments in Geochemistry*, Vol. 2, Elsevier, Amsterdam, 63-114. <https://doi.org/10.1016/b978-0-444-42148-7.50008-3>
- [34] Müller, D., Rock, N.M.S. and Groves, D.I. (1992) Geochemical Discrimination between Shoshonitic and Potassic Volcanic Rocks in Different Tectonic Settings: A Pilot Study. *Mineralogy and Petrology*, **46**, 259-289. <https://doi.org/10.1007/BF01173568>
- [35] Harris, C., Marsh, J.S. and Milner, S.C. (1999) Petrology of the Alkaline Core of the Messum Igneous Complex, Namibia: Evidence for the Progressively Decreasing Effect of Crustal Contamination. *Journal of Petrology*, **40**, 1377-1397. <https://doi.org/10.1093/petrology/40.9.1377>
- [36] Martin, H. (1993) The Mechanisms of Petrogenesis of the Archaean Continental Crust—Comparison with Modern Processes. *Lithos*, **30**, 373-388. [https://doi.org/10.1016/0024-4937\(93\)90046-F](https://doi.org/10.1016/0024-4937(93)90046-F)
- [37] Cullers, R.L. and Graf, J.L. (1984) Rare Earth Elements in Igneous Rocks of the Continental Crust: Intermediate and Silicic Rocks—Ore Petrogenesis. In: *Developments in Geochemistry*, Vol. 2, Elsevier, Amsterdam, 275-316. <https://doi.org/10.1016/B978-0-444-42148-7.50013-7>
- [38] Liégeois, J.P., Navez, J., Hertogen, J. and Black, R. (1998) Contrasting Origin of Post-Collisional High-K Calc-Alkaline and Shoshonitic versus Alkaline and Peralkaline Granitoids. The Use of Sliding Normalization. *Lithos*, **45**, 1-2. [https://doi.org/10.1016/S0024-4937\(98\)00023-1](https://doi.org/10.1016/S0024-4937(98)00023-1)
- [39] Kwékam, M., Talla, V., Fozing, E.M., Tcheumenak Kouémo, J., Dunkl, I. and Njonfang, E. (2020) The Pan-African High-K I-Type Granites from Batié Complex, West Cameroon: Age, Origin, and Tectonic Implications. *Frontiers in Earth Science*, **8**, Article No. 363. <https://doi.org/10.3389/feart.2020.00363>
- [40] Etheridge, M.A. and Coope, J.A. (1981) Rb/Sr Isotopic and Geochemical Evolution of a Recrystallized Shear (Mylonite) Zone at Broken Hill. *Contributions to Mineralogy and Petrology*, **78**, 74-84. <https://doi.org/10.2307/j.ctvc77m52.94>
- [41] Peter Gromet, L. and Silver, L.T. (1983) Rare Earth Element Distributions among Minerals in a Granodiorite and Their Petrogenetic Implications. *Geochimica et Cosmochimica Acta*, **47**, 925-939. [https://doi.org/10.1016/0016-7037\(83\)90158-8](https://doi.org/10.1016/0016-7037(83)90158-8)
- [42] Sawka, W.N. and Chappell, B.W. (1988) Fractionation of Uranium, Thorium and Rare Earth Elements in a Vertically Zoned Granodiorite: Implications for Heat Production Distributions in the Sierra Nevada Batholith, California, U.S.A. *Geochimica et Cosmochimica Acta*, **52**, 1131-1143. [https://doi.org/10.1016/0016-7037\(88\)90267-0](https://doi.org/10.1016/0016-7037(88)90267-0)

- [43] Romick, J.D., Kay, S.M. and Kay, R.W. (1992) The Influence of Amphibole Fractionation on the Evolution of Calc-Alkaline Andesite and Dacite Tephra from the Central Aleutians, Alaska. *Contributions to Mineralogy and Petrology*, **112**, 101-118. <https://doi.org/10.1007/BF00310958>
- [44] Miller, C.F., McDowell, S.M. and Mapes, R.W. (2003) Hot and Cold Granites: Implications of Zircon Saturation Temperatures and Preservation of Inheritance. *Geology*, **31**, 529-532. [https://doi.org/10.1130/0091-7613\(2003\)031<0529:HACGIO>2.0.CO;2](https://doi.org/10.1130/0091-7613(2003)031<0529:HACGIO>2.0.CO;2)
- [45] Miller, C.F. and Mittlefehldt, D.W. (1982) Depletion of Light Rare-Earth Elements in Felsic Magmas. *Geology*, **10**, 129-133. [https://doi.org/10.1130/0091-7613\(1982\)10<129:DOLREI>2.0.CO;2](https://doi.org/10.1130/0091-7613(1982)10<129:DOLREI>2.0.CO;2)
- [46] Lee, C.T.A. and Morton, D.M. (2015) High Silica Granites: Terminal Porosity and Crystal Settling in Shallow Magma Chambers. *Earth and Planetary Science Letters*, **409**, 23-31. <https://doi.org/10.1016/j.epsl.2014.10.040>
- [47] Rollinson, H.R. (2014) Using Geochemical Data. Routledge, London. <https://doi.org/10.4324/9781315845548>
- [48] Davidson, J., Turner, S., Handley, H., Macpherson, C. and Dosseto, A. (2007) Amphibole “Sponge” in Arc Crust? *Geology*, **35**, 787-790. <https://doi.org/10.1130/G23637A.1>
- [49] Macpherson, C.G. (2008) Lithosphere Erosion and Crustal Growth in Subduction Zones: Insights from Initiation of the Nascent East Philippine Arc. *Geology*, **36**, 311-314. <https://doi.org/10.1130/G24412A.1>
- [50] Cocherie, A. (1986) Systematic Use of Trace Element Distribution Patterns in Log-Log Diagrams for Plutonic Suites. *Geochimica et Cosmochimica Acta*, **50**, 2517-2522. [https://doi.org/10.1016/0016-7037\(86\)90034-7](https://doi.org/10.1016/0016-7037(86)90034-7)
- [51] Jung, S., Masberg, P., Mihm, D. and Hoernes, S. (2009) Partial Melting of Diverse Crustal Sources-Constraints from Sr-Nd-O Isotope Compositions of Quartz Diorite-Granodiorite-Leucogranite Associations (Kaoko Belt, Namibia). *Lithos*, **111**, 236-251. <https://doi.org/10.1016/j.lithos.2008.10.010>
- [52] Gregory Shellnutt, J., Wang, C.Y., Zhou, M.F. and Yang, Y. (2009) Zircon Lu-Hf Isotopic Compositions of Metaluminous and Peralkaline A-Type Granitic Plutons of the Emeishan Large Igneous Province (SW China): Constraints on the Mantle Source. *Journal of Asian Earth Sciences*, **35**, 45-55. <https://doi.org/10.1016/j.jseaes.2008.12.003>
- [53] Hofmann, A.W. (1988) Chemical Differentiation of the Earth: The Relationship between Mantle, Continental Crust, and Oceanic Crust. *Earth and Planetary Science Letters*, **90**, 297-314. [https://doi.org/10.1016/0012-821X\(88\)90132-X](https://doi.org/10.1016/0012-821X(88)90132-X)
- [54] Harris, N.B.W. and Inger, S. (1992) Trace Element Modelling of Pelite-Derived Granites. *Contributions to Mineralogy and Petrology*, **110**, 46-56. <https://doi.org/10.1007/BF00310881>
- [55] Condie, K.C. (1993) Chemical Composition and Evolution of the Upper Continental Crust: Contrasting Results from Surface Samples and Shales. *Chemical Geology*, **104**, 1-37. [https://doi.org/10.1016/0009-2541\(93\)90140-E](https://doi.org/10.1016/0009-2541(93)90140-E)
- [56] Eby, G.N. (1992) Chemical Subdivision of the A-Type Granitoids: Petrogenetic and Tectonic Implications. *Geology*, **20**, 641-644. [https://doi.org/10.1130/0091-7613\(1992\)020<0641:CSOTAT>2.3.CO;2](https://doi.org/10.1130/0091-7613(1992)020<0641:CSOTAT>2.3.CO;2)
- [57] Rudnick, R.L. and Fountain, D.M. (1995) Nature and Composition of the Continental Crust: A Lower Crustal Perspective. *Reviews of Geophysics*, **33**, 267-309. <https://doi.org/10.1029/95RG01302>

- [58] Barth, M.G., McDonough, W.F. and Rudnick, R.L. (2000) Tracking the Budget of Nb and Ta in the Continental Crust. *Chemical Geology*, **165**, 197-213. [https://doi.org/10.1016/S0009-2541\(99\)00173-4](https://doi.org/10.1016/S0009-2541(99)00173-4)
- [59] Rudnick, R.L. and Gao, S. (2003) Composition of the Continental Crust. *Chemical Geology*, **145**, 1-64.
- [60] Roberts, M.P. and Clemens, J.D. (2016) Origin of High-Potassium, Calc-Alkaline, I-Type Granitoids. *Geology*, **21**, 825-828.
- [61] Patiño Douce, A.E. (2000) What Do Experiments Tell Us about the Relative Contributions of Crust and Mantle to the Origin of Granitic Magmas? *Geological Society, London, Special Publications*, **168**, 55-75. <https://doi.org/10.1144/GSL.SP.1999.168.01.05>
- [62] Sylvester, P.J. (1998) Post-Collisional Strongly Peraluminous Granites. *Lithos*, **45**, 29-44. [https://doi.org/10.1016/S0024-4937\(98\)00024-3](https://doi.org/10.1016/S0024-4937(98)00024-3)
- [63] Moyen, J.F. (2009) High Sr/Y and La/Yb Ratios: The Meaning of the “Adakitic Signature”. *Lithos*, **112**, 556-574. <https://doi.org/10.1016/j.lithos.2009.04.001>
- [64] Helz, R. (1973) Phase Relations of Basalts in Their Melting Range at $\text{PH}_2\text{O} = 5$ kb as a Function of Oxygen Fugacity Part I. Mafic Phases. *Journal of Petrology*, **14**, 249-302. <https://petrology.oxfordjournals.org/>
- [65] Jung, S. and Pfänder, J.A. (2007) Source Composition and Melting Temperatures of Orogenic Granitoids: Constraints from $\text{CaO}/\text{Na}_2\text{O}$, $\text{Al}_2\text{O}_3/\text{TiO}_2$ and Accessory Mineral Saturation Thermometry. *European Journal of Mineralogy*, **19**, 859-870. <https://doi.org/10.1127/0935-1221/2007/0019-1774>
- [66] El Amrani, I.E., El Mouraouah, A. and Haimeur, J. (1992) Origine et signification des enclaves microgrenues sombres gabbroiques de la granodiorite des Oulad Ouaslam (Jebilet-Maroc). *Bulletin de l'Institut Scientifique, Rabat*, No. 16, 8-14.
- [67] Weyer, S., Münker, C. and Mezger, K. (2003) Nb/Ta, Zr/Hf and REE in the Depleted Mantle: Implications for the Differentiation History of the Crust-Mantle System. *Earth and Planetary Science Letters*, **205**, 309-324. [https://doi.org/10.1016/S0012-821X\(02\)01059-2](https://doi.org/10.1016/S0012-821X(02)01059-2)
- [68] Huang, H., Niu, Y., Zhao, Z., Hei, H. and Zhu, D. (2011) On the Enigma of Nb-Ta and Zr-Hf Fractionation—A Critical Review. *Journal of Earth Science*, **22**, 52-66. <https://doi.org/10.1007/s12583-011-0157-x>
- [69] Pearce, J. (1996) Source of Granitic Rocks. *Episodes*, **19**, 120-125.
- [70] Pearce, J.A., Harris, N.B.W. and Tindle, A.G. (1984) Trace Element Discrimination Diagrams for the Tectonic Interpretation of Granitic Rocks. *Journal of Petrology*, **25**, 956-983. <https://petrology.oxfordjournals.org/>
- [71] Maniar, P.D. and Piccoli, P.M. (1989) Geological Society of America Bulletin Tectonic Discrimination of Granitoids Subscribe Tectonic Discrimination of Granitoids. *GSA Bulletin*, **101**, 635-643. [https://doi.org/10.1130/0016-7606\(1989\)101<0635](https://doi.org/10.1130/0016-7606(1989)101<0635)
- [72] Harris, N.B.W., Pearce, J.A. and Tindle, A.G. (1986) Geochemical Characteristics of Collision-Zone Magmatism. *Geological Society, London, Special Publications*, **19**, 67-81. <https://doi.org/10.1144/GSL.SP.1986.019.01.04>
- [73] Affaton, P., Kröner, A. and Seddoh, K.F. (2000) Pan-African Granulite Formation in the Kabye Massif of Northern Togo (West Africa): Pb-Pb Zircon Ages. *International Journal of Earth Sciences*, **88**, 778-790. <https://doi.org/10.1007/s005310050305>
- [74] Barbarin, B. (1990) Granitoids: Main Petrogenetic Classifications in Relation to Origin and Tectonic Setting. *Geological Journal*, **25**, 227-238.

<https://doi.org/10.1002/gj.3350250306>

- [75] Tindle, A.G. and Pearce, J.A. (1981) Petrogenetic Modelling of *in Situ* Fractional Crystallization in the Zoned Loch Doon Pluton, Scotland. *Contributions to Mineralogy and Petrology*, **78**, 196-207. <https://doi.org/10.1007/BF00373781>
- [76] Bernard-Griffiths, J., Peucat, J.J. and Ménot, R.P. (1991) Isotopic (RbSr, UPb and SmNd) and Trace Element Geochemistry of Eclogites from the Pan-African Belt: A Case Study of REE Fractionation during High-Grade Metamorphism. *Lithos*, **27**, 43-57. [https://doi.org/10.1016/0024-4937\(91\)90019-H](https://doi.org/10.1016/0024-4937(91)90019-H)
- [77] Duclaux, G., Ménot, R.P., Guillot, S., Agbossoumondé, Y. and Hilairet, N. (2006) The Mafic Layered Complex of the Kabyé Massif (North Togo and North Benin): Evidence of a Pan-African Granulitic Continental Arc Root. *Precambrian Research*, **151**, 101-118. <https://doi.org/10.1016/j.precamres.2006.08.012>
- [78] Hoepffner, C. (1987) La tectonique hercynienne dans l'Est du Maroc. Thèse, Univ. Louis Pasteur, Louis, 295 p. <https://theses.hal.science/tel-01340643>
- [79] Lameyre, A., Black, J., Bowder, R. and Giret, P. (1984) Geology of Granites and Their Metallogenic Relations. Nanjing University, Science Press, Nanjing, 241-253.
- [80] Huppert, H.E. and Sparks, R.S.J. (1988) The Generation of Granitic Magmas by Intrusion of Basalt into Continental Crust. *Journal of Petrology*, **29**, 599-624. <https://doi.org/10.1093/petrology/29.3.599>
- [81] Turner, S., Sandiford, M. and Foden, J. (1992) Some Geodynamic and Compositional Constraints on "Postorogenic" Magmatism. *Geology*, **20**, 931-934. [https://doi.org/10.1130/0091-7613\(1992\)020<0931:SGACCO>2.3.CO;2](https://doi.org/10.1130/0091-7613(1992)020<0931:SGACCO>2.3.CO;2)
- [82] Attoh, B., Hawkins, K., Bowring, D. and Allen, S.A. (1991) U-Pb Zircon Ages of Gneisses from the Pan-African Dahomeyide Orogen, West Africa. *Eos Transactions American Geophysical Union*, **72**, 299.